

Soft-Surface Grasping: Radular Opening in *Aplysia californica*

Catherine E. Kehl¹, Joey Wu¹, Sisi Lu¹, David M. Neustadter⁴, Richard F. Drushel¹, Rebekah K. Smoldt¹, and Hillel J. Chiel^{1,2,3}

¹Biology, ²Neurosciences, ³Biomedical Engineering, Case Western Reserve University, ⁴Cardiac Success Ltd., Yokneam, Israel

Corresponding author's email address:

hjc@case.edu

Key words:

Feeding, molluscan behavior, soft body biomechanics

Summary statement:

Newly-described muscle fibers control a soft, flexible surface that the marine slug *Aplysia californica* uses to feed on seaweed, suggesting a novel mechanism for constructing a soft grasping device.

Abstract

Grasping soft, irregular material is challenging both for animals and robots. The feeding systems of many animals have adapted to this challenge. In particular, the feeding system of the marine mollusk, *Aplysia californica*, a generalist herbivore, allows it to grasp and ingest seaweeds of varying shapes, textures and toughness. On the surface of *Aplysia*'s grasper is a structure known as the radula, a thin flexible cartilaginous sheet with fine teeth. Previous *in vitro* studies suggested that an intrinsic muscle, I7, is responsible for opening the radula. Lesioning I7 *in vivo* does not prevent animals from grasping and ingesting food. New *in vitro* studies demonstrate that a set of fine muscle fibers on the ventral surface of the radula – the *sub-radular fibers* (SRFs) – mediate opening movements even if the I7 muscles are absent. Both *in vitro* and *in vivo* lesions demonstrate that removing the sub-radular fibers leads to profound deficits in radular opening, and significantly reduces feeding efficiency. A theoretical biomechanical analysis of the actions of the sub-radular fibers suggests that they induce the radular surface to open around a central crease in the radular surface and to arch the radular surface, allowing it to softly conform to irregular material. A three-dimensional model of the radular surface, based on *in vivo* observations and magnetic resonance imaging of intact animals, provides support for the biomechanical analysis. These results suggest how a soft grasper can work during feeding, and suggest novel designs for artificial soft graspers.

Introduction

Aplysia californica is a generalist herbivore that feeds on red, green and brown seaweeds (Winkler and Dawson, 1963; Kupfermann and Carew, 1974; Carefoot, 1987) that differ biomechanically. Red seaweeds *Laurencia pacifica* and *Gigartina canaliculata* have fern-like branching blades. Brown seaweed *Macrocystis pyrifera* (giant kelp) has blades that form large, leaf-like structures (laminae) supported by air-filled bladders. Green seaweed *Ulva lactuca* (sea lettuce) forms large sheets. Thus, unlike snails that rasp algae, *Aplysia*'s feeding apparatus must grasp and tear off pieces of seaweed whose shapes, toughness, and texture vary significantly, even within a single seaweed (Howells, 1942; Carefoot, 1987). The blades and the stipe supporting them may differ in their dimensions, calcification and chemical defenses (Hay, 1997), posing ongoing biomechanical challenges.

The biomechanics and neural control of feeding in *Aplysia* have been studied intensively (Chiel, 2007). As animals attempt to grasp food, they protract their tongue-like radula (a flexible cartilaginous soft surface covered with fine teeth), closing the radular surface near the peak of protraction (Kupfermann, 1974). A *biting* behavior is an attempt to grasp food that does not succeed; a *swallowing* behavior occurs when an animal does successfully grasp food and draws it into the buccal cavity (Kupfermann, 1974). As mechanical load increases, animals increase the force that they exert on seaweed, attempting to break off ingestible pieces (Hurwitz and Susswein, 1992). If an animal swallows material that it cannot ingest, or if the mechanical load becomes excessive, it repositions, releases, or ejects material (*rejection*), a behavior important for feeding efficiency (Katzoff et al., 2006).

Key muscles and motor neurons controlling the feeding apparatus of *Aplysia* (the buccal mass) have been described. *Protraction* of the grasper, which consists of the radular surface and the underlying musculature of the odontophore (the I4 and I6 muscles, and the cartilaginous, fluid-filled bolsters; Howells 1942) is mediated by the thin I2 muscle, which is innervated by motor neurons B31, B32, B61 and B62 (Hurwitz et al., 1996). Grasper *retraction* is mediated by the jaw (the I1/I3 muscles and the underlying jaw cartilage) whose contractions are induced by the B6, B9, B10 and B3 motor neurons (Morton and Chiel, 1993; Lu et al., 2015), and by the hinge muscle (the interdigitation of the I2 muscle, the I1/I3 muscle, and the major muscle of the odontophore, I4), whose force is generated by the B7 motor neuron (Sutton et al., 2004a; Ye et al., 2006). Radular *closing* is mediated by the horseshoe-shaped I4 muscle, which is innervated

by the B8a and B8b motor neurons (Morton and Chiel, 1993). *In vitro* studies suggest that grasper *opening* is mediated by the I7 muscles that are primarily innervated by the B48 motor neurons (Evans et al., 1996).

Visualizing movements of the internal structures of the feeding apparatus using magnetic resonance imaging (MRI) in intact animals provided important insights into biting, swallowing and rejection (Neustadter et al., 2002a; 2007; Novakovic et al., 2006). A kinematic model based on the MRI studies quantified feeding movements (Neustadter et al., 2002b; 2007), and kinetic models quantified muscle forces during feeding (Sutton et al., 2004b; Novakovic et al., 2006). These models did not incorporate the internal details of the grasper, i.e., the radular surface and the underlying odontophore. Thus, we sought to understand the *in vivo* opening of the radular surface by developing a novel surgical approach to lesion muscles beneath the radular surface, and to create a more detailed three-dimensional model of the process of opening, based in part on the MRI data, using a program that can represent forces acting on a soft surface.

We discovered that I7 plays a role radular opening, but previously undescribed muscles, the *sub-radular fibers* (SRFs), also mediate opening and arching of the radular surface, which is critical for the ability of the surface to softly conform to irregular seaweed shapes. Lesions of I7 or of the sub-radular fibers significantly reduce radular opening and arching; SRF lesions significantly reduce swallowing efficiency. A theoretical biomechanical analysis predicts how the sub-radular fibers may control the radular surface, and a three-dimensional model supports the predictions of the biomechanical analysis. These results have implications for molluscan herbivory, and suggest novel approaches for creating soft-surface graspers.

Materials and methods

Animals

Adult *Aplysia californica* (250 - 400 g) were obtained from South Coast Bio-Marine, San Pedro, CA, and Marinus Scientific, Long Beach, CA. Animals were maintained in aerated 189 L aquaria containing artificial seawater (Instant Ocean Spectrum Brands, Blacksburg, VA) at a temperature of $16^{\circ}\text{C} \pm 1^{\circ}\text{C}$. Animals were fed 150 cm² of seaweed (dried Nori (Sushi-Nori, Nagai Nori Co, Ltd. Torrance, CA) or Dulse (Natural Zing LLC, Mount Airy, MD)) every other

day. To ensure that animals used for these studies were healthy, a small piece of seaweed was presented, and animals that generated normal inter-bite intervals (3 - 5 seconds; Kupfermann, 1974) were selected for use.

***In vitro* preparation**

The *in vitro* preparation was based on that developed for prior studies of the role of the I7 muscle in opening (Evans et al., 1996; a schematic view of the feeding apparatus within the animal is shown in Figure 1A, the main muscles of the feeding apparatus are shown in Figure 1B, and the location of the I7 muscle is shown schematically in a lateral cutaway view in Figure 1C). Animals were anesthetized with an injection of isotonic magnesium chloride equal to their body weight, and the buccal mass was dissected out. An incision through the dorsal midline of the jaws and esophagus exposed the radula and odontophore. The surface of the radula was gently peeled away from the underlying I4/bolster musculature, and the muscles attaching the radular surface to the odontophore were also severed: I6, I7, I8, I9 and I10 (Evans et al., 1996).

The preparation was placed in *Aplysia* saline (460 mM NaCl, 10 mM KCl, 22 mM MgCl₂, 33 mM MgSO₄, 10 mM CaCl₂, 10 mM glucose, and 10 mM MOPS, pH 7.5). For the control group, the non-hydrolyzable cholinergic agent carbachol (Sigma; final concentration 4 mM) was applied to the solution to induce motor movements (Susswein et al., 1996), which were recorded with a video camera. In the experimental preparations, either both I7 muscles, the sub-radular fibers, or the I7 muscles and the sub-radular fibers were lesioned (see section on *in vivo* lesion for further details on lesions of the sub-radular fibers). Since the I7 muscle and the sub-radular fibers were completely exposed, there was no need to make any incision in the radular surface to access them. Carbachol was added to the bath and the resulting movements were recorded on video.

Histological analysis of the sub-radular fibers

Once the sub-radular fibers were identified in the *in vitro* preparations, we examined them histologically (Conn 1953). All reagents were obtained from Fisher Scientific. Macroscopic observations of the sub-radular muscle fibers *in situ* were done by gently brushing them with a dilute solution of toluidine blue (0.1% in *Aplysia* saline). To obtain stains of the deeper fibers, the surface was covered in a solution of 0.5 % w/v toluidine blue in *Aplysia* saline

and left to stain for ten minutes before washout. Fibers were then photographed using an SMZ-171-TLED Stereo Microscope system with a T2 tablet camera (Motic Optical, North America). To visualize the microscopic structure of the fibers, the buccal mass was dissected out from a 50 g *Aplysia* after anesthesia by intra-cavity injection of cold (4 °C) 333 mM aqueous MgCl₂, then fixed in 10% v/v aqueous phosphate-buffered formalin for one week at room temperature (25 °C). Excess lip and esophagus tissue were trimmed away, leaving a final specimen approximately 6.6 mm in antero-posterior length. Subsequent processing for histology used standard techniques as described in Humason (1969). Following overnight rinse in running tap water, the buccal mass was dehydrated in graded ethanols, cleared in xylene, embedded in Paraplast, and serially-sectioned perpendicular to the antero-posterior axis at 20 μm. Sections were mounted on Haupt's gelatin-coated slides, dried overnight at 45 °C, stained with Mallory's Heidenhain hematoxylin, and coverslipped with Permount. Entire sections were photographed at low power using a Wild M3Z stereo dissection microscope, whereas high-resolution details were photographed using a Zeiss compound microscope.

***In vivo* surgery**

After the animal's mass was measured, animals were anesthetized by injecting an amount of isotonic magnesium chloride (333 mM) equal to about a third of their body weight, and allowed to relax completely. The buccal mass, which can be palpated through the skin when the animal is fully relaxed (Figure 1A), was gently massaged until it was against the jaws. Gentle pressure was used to push the radular surface and the underlying odontophore through the jaws, taking care to not fully evert the buccal mass, which would cause significant muscle damage, from which the animal would take considerable time to recover (Figures 1B and 1C show the internal anatomy of the muscles surrounding the radular surface). An incision was made in the base of the radula (the side nearest the prow; Figure 1B) in the mid-sagittal plane (Figure 1D). Surgical manipulations were applied through this hole in the radular surface. Sham lesioned animals received this radular incision but no underlying muscles were removed.

To lesion the I7 muscles, the two I7 muscles were identified on either side of the incision, and pulled up through the incision (Figure 1E). The muscles were carefully disconnected from their upper locations on the underside of the radular surface on either side of the incision, and then pulled upwards so that they could be snipped off at their base near the base of the radular

stalk to ensure that they could not re-attach or re-generate during the recovery period. To remove sub-radular fibers, a scalpel was inserted through the incision, and the sub-radular fibers were carefully removed from the underside of the ventral radular surface around the crease in the radular surface (Figure 1F; note inset). To avoid excessive damage to the radular surface, only those fibers in the immediate vicinity of the surface incision were removed. Based on post-mortem examination, we estimate that about two-thirds of the sub-radular fibers were removed. Because the innervation of these muscles has not yet been determined, it was not feasible to denervate them and determine the effects of their passive properties alone.

After surgery, animals were allowed to recover in an isolated aerated small tank suspended within the larger aquarium, and were tested for their ability to feed for up to a week after surgery. Animals that did not recover after a week were not included in the study.

Behavioral measurements

Animals were selected for studies based on their motivation to feed. Using the same criterion established by Kupfermann (1974), we selected animals that generated several bites whose inter-bite intervals were between 3 to 5 seconds. Bites were obtained after animals had been aroused to feed, and were selected for analysis based on their visibility in the video recordings, and the extent to which they were perpendicular to the camera's view.

To the extent possible, blinding was done by not informing the investigator who performed the behavioral tests or who analyzed the data which lesion had been done, or whether an animal had only received a sham lesion.

Normalized width measurements: Peak opening width was measured in intact animals before surgery and then on the first day animals were able to bite after surgery (up to a week post-surgery). Animals were placed in a beaker of artificial seawater and were induced to generate strong bites such that the plane formed by the jaws was parallel to the plane of focus of the video camera by applying small pieces of seaweed to the inner surfaces of the anterior tentacles, near the perioral zone (Figure 2A). Behavior was recorded on video using a Logitech QuickCam Vision Pro Webcam. Opening width has previously been shown to correlate well with the magnitude of odontophore protraction (Neustadter et al., 2002a). Bites were obtained from each animal prior to and after the lesion (sham lesion, I7 lesion, SRF lesion, or I7 and SRF lesion, referred to as a dual lesion). Measurements of opening were done from the video

recording at the peak of bites. The peak of the bite was determined by a frame-by-frame analysis to determine the exact frame at which peak protraction occurred.

To compare animals, measures of opening width were normalized. The width was measured perpendicular to the axis formed by the radular cleft, $2/3$ from the inner surface of the radular base (Figure 2B). Normalization was performed by taking the ratio of peak opening width to the length (the distance from the inner surface of the radular base to the cleft-side edges of the radular surface; Figure 2B). The same normalized measure of opening width was used to quantify the openings in the *in vitro* preparation, and in the model.

Normalized measurements of radular curvature: During the initial protraction phase of a bite, the radular surface in normal animals shows a clear, gentle curvature, which allows it to conform to the irregular shapes of seaweed; as the radula closes, a sharp ridge forms around the central crease in the radular surface, allowing animals to firmly grasp and pull seaweed inward (see Figure 2C). A direct measurement of the surface curvature would be extremely difficult, even with two cameras, because the animal has no hard body parts to which cameras could be anchored, and moves considerably during biting behavior. Instead, since the ridge that forms at the peak of protraction during biting completely excludes an area of gentle curvature, and it generates a very characteristic inflection point that can be seen even in single camera views, we chose to measure the percentage of the surface occupied by the ridge as a proxy for the radular surface curvature. The width of the ridge was normalized by the total width of the radula (see Figure 2C). Animals served as their own controls; four bites were obtained before and after surgery, and the difference in the mean normalized length occupied by the ridge was computed for each animal.

Feeding efficiency measurements: To determine the functional effect of lesions on the actual feeding behavior of animals, their ability to swallow seven uniformly-sized strips of seaweed (Nori, 1 cm by 3 cm strips) was measured. As a measure of feeding efficiency, the number of swallows that the animal required to ingest the strip was measured. Animals were used as their own controls, and the difference in the mean number of swallows before and after surgery was computed for each animal, normalized by the mean number of swallows prior to surgery. Although we attempted to quantify feeding efficiency in animals subjected to dual I7 and SRF lesions, their inability to grasp and hold food made this extremely difficult. It should be noted that this indicates that the dual lesions severely reduce feeding efficiency.

Statistical analyses

For the *in vitro* experiments, in which animals could not serve as their own controls, we used G*power 3.1 (freely available at <http://www.gpower.hhu.de> (Faul et al. 2009)) to determine the size of the groups for analysis of variance (power of 0.95, 4 groups (i.e., sham, I7 lesion, SRF lesion, and dual lesion groups), α value of 0.05, an effect size of 0.1 standard deviations), and found that an N of 6 per group would be sufficient. Bartlett's test showed no significant difference in variance (heteroscedasticity). One-way ANOVA was used to determine overall effects of the lesions, and post-hoc Tukey tests were done to determine the significance of the individual lesions.

For the *in vivo* data (change in opening percentage, change in ridge formation, and feeding efficiency), animals served as their own controls. Using G*Power 3.1, we determined that for an α level of 0.05, and an effect size of -0.2 ± 0.1 (determined from pilot studies), we would obtain a power ($1 - \beta$) of 0.97 for N = 5, and a power of 0.91 for N = 4 for a paired t-test. To perform ANOVA with the same significance and power levels would have required up to 5 times as many animals per group according to G*Power 3.1, so we compared magnitudes of effects by computing *effect size* [Chow et al. 2008]: mean of the differences divided by the standard deviation of the differences.

For the opening percentages and the ridge formation, mean values before and after the lesions (sham lesion, I7 lesion, SRF lesion, or both I7 and SRF lesions) were subtracted to obtain a single paired difference in opening percentage for each animal. For the feeding efficiency measures, mean number of swallows (on seven strips of Nori) before and after the lesions were subtracted, and divided by the mean number of swallows before the lesion to obtain a single paired normalized feeding efficiency for each animal. For the sham, I7, and SRF lesion groups, we used an N of 5. Because of the difficulty of doing combined SRF and I7 lesions, we only used an N of 4 for opening measures and an N of 3 for ridge formation. Because dual lesion animals fed very poorly, as mentioned above, we did not obtain feeding efficiency measures from them.

Prior to performing a paired t-test, we tested for the normality of the differences using the Kolmogorov-Smirnov test, setting the critical value for the test to $p = 0.05$. All the data satisfied this test for normality. A one-tailed paired t-test was applied with a critical value of 0.05 because

we expected that the lesions would decrease opening percentage. Since each animal served as its own control, and the four groups were independent of one another (i.e., sham, I7 lesion, SRF lesion, and dual lesion), no corrections were needed for multiple comparisons.

Model

To test biomechanical hypotheses about the functions of the sub-radular fibers during opening, and the consequences of lesioning them, a computational model was constructed. First, a detailed, static, three-dimensional model of sub-radular structures thought to contribute to radular movements was made (Figure 3A; high-spatial-resolution data from Neustadter et al., 2002a; spatial resolution was 0.1 mm by 0.1 mm). Anatomical studies allowed determination of the radular shape while intact (Figure 3B). The initial configuration of the sheet-like radular surface was based on its flattened shape after it was peeled away from the underlying I4 muscles/bolsters (schematically shown in Figure 3C). The key structures (the I4 muscles and the cartilaginous bolsters within them, and the I6 muscle – see Neustadter et al., 2002b) that contributed to the shape of the surface within the detailed static model are shown in Figure 3D. These were somewhat simplified for computational efficiency (Figure 3E; note, for example, the significant simplification of the shape of the I4/I6 complex).

A three-dimensional model that could capture both movements (kinematics) and forces (kinetics) was assembled from these components using the open source Blender modeling and animation environment (www.blender.org, v.2.77a). The I4/bolsters and I6 muscles were represented with a single mesh object (Figure 3E and 3G, red; in 3G, the posterior edge of the I4/I6 complex is labeled I6, since that is the location of the I6 muscle). The radular surface (Figure 3E) and radular sac (Figure 3D and 3E) were each represented with separate mesh objects.

When the flattened surface of the radula was attached to the edge of the bolsters, which is anatomically correct (Supplementary Figure 1A, leftmost image; Figure 3G), it was possible to deform the soft surface so that it would accept the radular sac without creating significant collisions between their respective meshes. Insertion of the radular sac mesh is shown in sequence until the surface was complete (rightmost image, Supplementary Figure 1E). The final surface configuration (Figure 3E) was similar to that observed in the animal (Figure 3B and 3D).

To ensure the correctness of the kinematics of the underlying structures, which determine the actual deformations of the radular surface during biting, the positions of the radular sac, the margin of the I6 muscle, and the orientation of the I4/bolsters were determined by carefully analyzing single frames of high-temporal-resolution MRI images (Figure 3F; mid-sagittal images were acquired every 310 ms at a spatial resolution of 1 mm by 1 mm; details of the MRI protocol for obtaining the images are described in Neustadter et al., 2002a; 2007). Once these structures were positioned (Figure 3G), the edges of the radular surface could be correctly constrained and positioned (Figure 3G, blue line). Thus, the movements of the underlying structures could now determine the shape of the radular surface. The surface was simulated using a hybrid of the Blender Cloth Simulation Engine and the Bullet Physics Engine (<http://bulletphysics.org/wordpress/>), so that the shapes assumed by the surface were entirely determined by the movements of the underlying structures and the physical response of the soft surface.

The surface of the radula and the underlying sub-radular fibers were represented as a single mesh. All the vertices within the mesh were assigned values indicating the stiffness and ability of edges between them to bend. During the initial assembly phase, the entire mesh was assigned a relatively stiff value to assure that the entire surface would assume an appropriate configuration. After the assembly phase, the mesh as a whole was assigned a relatively low stiffness, so that it could easily bend and fold.

To represent the sub-radular muscle fibers, a group of vertices were defined (see Figure 3H, indicated in red). Within this vertex group, the values of stiffness could change during the course of a bite. During the time that the sub-radular fibers were active, this entire vertex group was assigned high stiffness. During the phase in which the sub-radular fibers were passive, these vertices were slightly stiffer than the background value of the rest of the mesh to capture the passive properties of the sub-radular fibers. The timing of activation of the model sub-radular fibers was based on the timing of activation determined from EMG measurements of sub-radular fiber activity.

To represent the lesion, vertices were removed from the vertex group, corresponding to the removal of the muscle fibers (see Figure 3I, indicated in red). The timing of activation of the model sub-radular fibers was otherwise identical to the control runs of the model.

To test the importance of the timing of the activation of the sub-radular fibers, the times that the model sub-radular fibers were activated were inverted: during the times that the sub-radular fibers would have been active, the values of the vertices were inactive (i.e., only slightly more stiff than the remainder of the mesh), and during the times that they would have been inactive, they were activated (i.e., much stiffer than the rest of the mesh).

Preliminary studies using EMG extracellular electrodes in an isolated buccal mass in which I7 and the SRF were intact indicated that the fibers were activated at times similar to the activation of the I7 muscle (data not shown), so the timing of stiffening corresponded to the timing of activity of the I7 muscle during biting (Evans et al., 1996). Because changing activation of the I7 muscles would alter the movements of the radular stalk, and we have no data on how the radular stalk moves in the absence of the I7 muscle, the model focused solely on how changing the activity of the sub-radular fibers altered the opening of the radular surface.

Results

***In vitro* studies of I7 identified a new source of opening movements: sub-radular fibers**

In vitro studies suggested that the I7 muscle was responsible for radular opening (Evans et al., 1996). The reduced preparation in which I7 was studied consisted of the radular surface dissected free from the underlying musculature (the I4, which contains the bolsters). To understand how the radular surface was controlled by the I7 muscle, we bilaterally lesioned them *in vitro* (see Methods; Figure 4A). To our surprise, the *in vitro* preparation continued to show strong openings, both spontaneously and in response to carbachol (Figure 4B, 4C (Control, I7 Lesion; these two groups are not significantly different)).

We therefore investigated other muscles that could generate opening, and discovered muscle fibers underlying the surface of the radula, which we termed the sub-radular fibers (SRF). As these fibers contracted, the radular surface opened. Since these fibers form a thin transparent sheet that might not generate significant force, we tested their role in opening by lesioning them. Lesions of the sub-radular fibers led to significant reductions in normalized opening widths *in vitro* in response to carbachol (Figure 4C, SRF Lesion). Lesioning both the subradular fibers and the I7 muscles led to similar significant deficits in opening (Figure 4C, Dual Lesion).

Anatomy and histology of the sub-radular fibers

The sub-radular fibers have not been previously described, so we characterized them anatomically and histologically. The reduced preparation could be flattened out (Figure 5A), and on the ventral side of the radular surface, surrounding a medial crease, fine muscular fibers extended from either side (Figure 5B). Histological studies (see Methods) revealed fibers that run longitudinally along the crease (Figure 5C, light staining; 5D, heavy staining; note white upper arrows); fibers course both laterally and perpendicular to the crease (Figure 5C, 5D; note white lower arrows). Serial sections through the buccal mass (20 μm thickness; Figure 5E) provided more detailed views. Low power views of the sections showed a clear region of muscle just beneath the cartilaginous surface of the radula (Figures 5F, 5G), and partial sections of the I7 muscles (Figure 5H). Higher magnifications (Figures 5I, 5J) showed a thin layer of tightly packed muscle fibers running longitudinally along the central radular crease, and fibers that also ran perpendicular to the radular crease (Figure 5J). The muscles showed no striations; rather, they resembled smooth muscle, as observed in many other molluscan species (Hooper and Thuma, 2005; Hooper et al., 2008).

***In vivo* lesions of I7 and the sub-radular fibers reduce radular opening and arching**

We focused on two behavioral features that are likely to be important to feeding: radular opening and arching. Radular opening was not significantly affected by the sham lesions, but was significantly reduced after bilateral I7 lesions (Figure 6A, Sham, I7 Lesion). Opening was significantly reduced by lesions of the sub-radular fibers and by lesioning both the sub-radular fibers and the I7 muscles (Figure 6A, SRF Lesion, Dual Lesion). Residual opening is probably due to the remaining sub-radular fibers near the base of the radular crease, since only about two-thirds of the sub-radular fibers were removed (see Methods). The data support the hypothesis that the sub-radular fibers, as well as the I7 muscles, contribute significantly to radular opening.

During early protraction, the radular surface curves gently, allowing it to conform to food. A proxy measure for radular curvature is the formation of the ridge around the crease, which excludes the region of gentle curvature (see Methods, and see below). Sham lesions slightly reduced the area not occupied by the ridge, but these reductions were not significant (Figure 6B, Sham). Bilateral lesions of the I7 muscles significantly reduced the area not occupied

by the ridge (Figure 6B, I7 Lesion). Lesions of the sub-radular fibers, or of both the I7 muscles and the sub-radular fibers, also significantly reduced the area not occupied by the ridge (Figure 6B, SRF Lesion, Dual Lesion). These data support the hypothesis that the sub-radular fibers, along with the I7 muscles, significantly contribute to the arching of the radular surface.

Feeding efficiency is significantly reduced by sub-radular fiber lesions

Deficits in grasper opening should reduce the ability to grasp and swallow food so that lesions of I7 or the SRF could cause swallowing deficits. Animals were fed with seven uniform seaweed strips, and the number of swallows necessary to ingest each strip were measured before and after lesions. Animals were used as their own controls to reduce variability. Animals subjected to both I7 and SRF lesions were difficult to feed; their feeding difficulty clearly indicated qualitatively that the dual lesions were effective in altering feeding. Animals subjected to sham lesions alone showed a significant increase in the number of swallows needed to ingest a strip (Figure 6C, Sham), perhaps because the sham lesion cuts through the region of the sub-radular fibers (Figure 1D). Animals subjected to SRF lesions required significantly larger numbers of swallows to ingest a strip than they did prior to surgery (Figure 6C, SRF Lesion). Although animals receiving an I7 lesion showed a trend towards requiring more swallows, the difference was just below the level of significance (Figure 6C, I7 Lesion). Thus, behavioral data support the hypothesis that the sub-radular fibers generate opening movements of the radula necessary for normal feeding behavior. I7 may also contribute, but its effects are difficult to separate from the effects of the sham lesions.

A biomechanical hypothesis for the actions of the subradular-fibers

The surface of the radula is critical during feeding. *Aplysia* grasp seaweed by their foot and anterior tentacles (Kupfermann, 1974), bringing it to the radular surface which conforms to the irregular shape of seaweed, exerting forces to pull pieces of seaweed inward and break them off. How do the subradular fibers and the I7 muscles (Figure 7A i and 7A ii) contribute to opening the radula and making its surface soft and deformable? A biomechanical analysis suggests testable hypotheses for the muscle functions.

Contraction of the sub-radular fibers applies compressive forces to the underside of the radular surface, inducing the upper surface to curve outwards (Figure 7B). As shown earlier, the radular surface has a central crease that, in the absence of muscular contractions, will tend to induce a fold in the surface (Figure 5A). Furthermore, the radular surface is quite flexible in response to compressive forces, but very stiff in response to tensile forces, showing almost no elastic expansion when subjected to tensile forces (HJC and CEK, unpublished observations). The crease creates an axis of local stiffness within the surface of the radula, so that when the sub-radular fibers contract, they cannot deform the tissue along the stiff axis of the crease. Instead, they curve the two surfaces on either side of the crease away from the central crease, inducing opening (Figure 7C i and 7C ii). Similarly, the I7 muscles can locally increase the curvature of the radular surface near the prow, applying compressive forces to the underside of the radular surface (Figure 7F i, 7F ii, and 7F iii), while at the same time moving the radular sac, and thus contribute to the outward curvature of the radular surface, inducing opening around the crease.

The sub-radular fibers also contribute to arching radular surface so that it can softly envelop irregularly-shaped seaweed. The arching of the yellow radular surface is readily visible from the outside of the animal during a bite (Figure 7D i and 7D ii). As the animal begins to retract the grasper, the shape of the surface changes, and strongly pinches together to form a ridge (Figure 7D iii). The ridge makes the radular surface rigid, and is not due I7 activation, since the I7s are active prior to and after the activation of the closer muscle for the grasper, I4 (see Neustadter et al. 2007, Figure 14A). Preliminary EMG measurements indicated that the SRF are active at the same time as the I7 muscles, so they are also not responsible for ridge formation. The fine teeth that line the radular surface face posteriorly, so the ridge helps anchor the teeth within the seaweed, at the same time that the pinched radular surface compresses the grasped seaweed, generating a strong grip that can tear off seaweed pieces.

A biomechanical analysis suggests how the sub-radular fibers may generate arching, and how cessation of their activity could lead to the radular ridge. Along its outer edge, the radular surface tightly adheres to the outer edge of the horseshoe-shaped I4 muscle (Figure 3B); along its inner edge, the radular surface is continuous with the radular stalk (Figure 3A). To induce opening, both the I6 and the I7 muscles can move the top of the radular surface close to the base of the radular stalk, pulling the radular sac between the halves of the radular surface. The radular

surface is then subjected to lateral compressive forces from the surrounding jaw cartilage and medial compressive forces from the radular sac (Figure 7E i). When the sub-radular fibers are activated, the bottom of the radular surface is subjected to compressive forces, inducing the top of the surface to arch upwards and generate tensile forces that resist the surrounding compressive forces (Figure 7E ii). To induce closing, the I4 muscle contracts, increasing the distance between the radular surface and the radular sac, which is attached to the base of the I4 muscle through the I8, I9 and I10 muscles (Evans et al., 1996). Initially, this allows the surfaces of the radula to come together medially. As the medial radular surface is pulled ventrally, if the sub-radular fibers cease to be active, no forces resist the pinching together of the top of the radular surface, resulting in its compressed, ridge-like appearance (Figure 7D iii, 8E iii). Thus, controlling sub-radular fiber activation may be important for the control of the soft radular surface.

Testing sub-radular fiber function using a three-dimensional model

A model tested the biomechanical role of the sub-radular fibers. Using high-spatial-resolution magnetic resonance imaging (MRI), the internal structures of the grasper were reconstructed. High-temporal-resolution MRI generated movies of the mid-sagittal view of the grasper during swallowing and biting (Neustadter et al., 2002a; 2007), and a three-dimensional kinematic model was previously created to determine the changes in muscle lengths during these movements (Neustadter et al., 2002b, 2007; see Methods for details of the spatial and temporal resolution of the MRI measurements). We simulated the movements of a soft surface using the open-source Blender animation program, linked to the physics simulator Bullet. The soft surface was anchored to the representations of the I4 muscle, the bolsters and the I6 muscle, and these structures that move the radular surface were induced to follow the same kinematic sequence observed during the MRI movies. Based on microscopic examination of flattened radular surfaces, we set up a coarse mesh to represent the columnar distribution of the teeth on the radular surface. This mesh allowed the surface to fold in ways similar to those observed in the isolated radular surface. The surface was not otherwise controlled by the model.

Elements representing the subradular fibers beneath the soft radular surface were stiffened in the locations on the radular surface and at the times that the data presented above suggest the fibers should be activated (see Methods). To capture the effect of lesions of the sub-

radular fibers, the elements were not stiffened beneath the model radular surface during the movements of the underlying structures.

When the fibers were stiffened, the surface showed a clear opening and arching of the radular surface (Figure 8A; compare with the *in vivo* peak protraction, Figure 8B). When they were not stiffened, the surface showed little opening (Figure 8C; compare with the *in vivo* peak protraction of an animal subjected to an SRF lesion, Figure 8D). We quantified these results by applying the same measurements of normalized opening width to the model, and found that the results were similar to those observed *in vivo* (the difference in the normalized open percentage was -0.46 , similar to the maximum effect of SRF lesions, -0.42). Applying the same measurements of change in normalized ridge formation to the model yielded smaller effects than those observed in animals after SRF lesions (a reduction of -0.17 ; the smallest effect of an SRF lesion was -0.35); this may be due to the inability to fully see the edge of the radular surface in intact animals. Changing the timing of the SRF activation greatly disrupted all aspects of the bite (data not shown).

Discussion

Grasping in *Aplysia* requires the radular surface to open and conform to irregular seaweed. Lesions of the I7 muscle lead to deficits in opening and in the ability of the radular surface to arch in intact, behaving animals (Figure 6A, B), but animals can still bite and swallow. Anatomical and behavioral studies suggest that an additional set of fibers running on the underside of the radular surface on either side of the radular crease, the *sub-radular fibers* (SRFs; Figure 5), can induce strong openings *in vitro* in the absence of the I7 muscles (Figure 4C). Lesions of the sub-radular fibers *in vivo* lead to significant deficits in the ability of animals to open and arch the radula (Figure 6A, B) and reduce feeding efficiency (Figure 6C). A biomechanical analysis of the sub-radular fibers (Figure 7) suggests that, when these fibers shorten along the underside of the radular surface, they induce arching and tension forces in the radular surface that resist compressive forces which would otherwise induce the surface of the radula to pinch together in a hard ridge. A simulation of soft-surface mechanics incorporating the

structures that move the radular surface supports the hypotheses that the sub-radular fibers control opening and maintain the arching of the radular surface (Figure 8).

Relative roles of I7 muscles and the sub-radular fibers

What are the relative roles of the I7 muscles and the sub-radular fibers in controlling opening of the radula? Lesions of the I7 muscles do induce significant deficits in opening width and arching *in vivo*, whereas lesions of the sub-radular fiber cause larger effects on opening and arching (Figure 6A, B). Lesioning both I7 and the sub-radular fibers does not induce an additive deficit in normalized opening width that is significantly larger than the deficit due to solely lesioning the sub-radular fibers (Figure 6A, B). The observation that lesions of the sub-radular fibers also reduce feeding efficiency (Figure 6C) strongly support the hypothesis that the sub-radular fibers are important for feeding behavior. It is likely that the I7 muscles are important for feeding, although lesions of I7 just failed to reach statistical significance (Figure 6C). If the I7 muscles play a role in positioning the radular stalk, then lesions of the I7 muscles might contribute to feeding efficiency even if they do not primarily mediate radular opening. Indeed, the I7 muscle is activated during multiple phases of biting and swallowing (Evans et al., 1996, Figure 4), and thus could affect both opening and closing (see also Figure 14A, B in Neustadter et al., 2007). That I7 could have multiple roles is not surprising. A study of the I5 muscle (also known as the accessory radula closer or ARC muscle) suggested that its effects on the radular surface depended on its mechanical context (Orekhova et al., 2001).

Radular function and molluscan herbivory

Understanding radular function in *Aplysia* is important for the comparative anatomy of radulae in different molluscan species, and the roles that *Aplysia* play in ocean ecology. Herbivory can significantly affect the distribution of benthic algae and induce a variety of changes in seaweed, including its distribution, chemical defenses, and calcification (Duffy and Hay, 1990). An influential study (Steneck and Watling, 1982) examined the relationship between radular morphology and diet, but omitted opisthobranch mollusks because (p. 300) “they use their feeding apparatus in a fundamentally different way and thus make comparisons with other herbivorous mollusks difficult.” As described by Howells (1942) and summarized by Carefoot (1987), during feeding, *Aplysia* tear off pieces of seaweed with their radula, and then grind it

within their gizzard (Carefoot, 1987). A combined field and experimental study by Pennings demonstrated that as *Aplysia* grow, their preferred diet can change (Pennings, 1990). Dietary changes may be due to the increased strength of the radula: chopped seaweed (*Codium*) allowed smaller animals to grow faster than the original whole seaweed (Pennings 1990). Comparative studies of several sea hares from the coast of Australia suggested that radular teeth complexity could determine diet: simpler teeth might be associated with a broader diet (e.g., the teeth of *Dolabella auricularis*), whereas more complex teeth might be associated with a more specialized diet (e.g., the teeth of *Stylocheilus striatus*) (Clarke, 2004). A complicating factor, however, is that opisthobranch molluscan morphology may be affected by the diet itself (Trowbridge, 1997). Indeed, a recent study in *Aplysia brasiliiana* showed that the molecular biology of related species was nearly identical, but there were significant differences in radular teeth morphology (de Olivera Saad et al., 2014). Studies of the radula have focused primarily on the teeth covering its surface. To our knowledge, there have been no studies of the dynamic changes of the flexible radular surface during feeding in *Aplysia californica*. Understanding the ability of the radular surface to envelop seaweed structures and apply high forces to tear off pieces of seaweed is likely to be important for understanding *Aplysia* herbivory and its implications for the growth and properties of benthic algae.

Use of small muscles to modulate the functions of large muscles

Small muscles can alter the effects of large muscles in multiple ways: changing the alignment or positioning of large muscles, triggering their actions, steering them, or positioning limbs through their passive properties. In the buccal mass, small muscles play a critical role in positioning larger muscles, thus affecting behavior. Relative to the volume of the I4 muscle, the bolsters, and the I6 muscle, the other muscles of the grasper are much smaller: the I7 muscles are two thin straps (Figure 3A); the sub-radular fibers are a thin sheet beneath the surface of the radula (Figure 5); and the I8, I9 and I10 muscles are very small muscles near the base of the radular stalk (Evans et al., 1996). Similarly, the I5 muscle (ARC) is a relatively small muscle that inserts along the radular stalk on one end, and on the outer surface of the I4 muscle at its other end (see Figure 21 of Neustadter et al., 2002b and Figure 2 of Neustadter et al., 2007). Despite their small size, these muscles play critical roles in controlling the radular surface relative to the I4/bolsters/I6 muscles. Similarly, the thin I2 muscle that covers the posterior surface of the

buccal mass, plays a critical role in protracting the grasper (Hurwitz et al., 1996), which has much larger volume than the I2 muscle. Another example is provided by the very small extrinsic muscles of the buccal mass (E1, E2, E3, E4, E5 and E6) that orient and position the entire buccal mass within the animal's head (Chiel et al., 1986). Despite their small size, lesions of the extrinsic muscles significantly reduce feeding efficiency (Chiel et al., 1986), similar to the effects of lesions of I7 and the sub-radular fibers.

Small muscles can affect the actions of much larger muscles through energy release, steering, and passive control mechanisms of limb position. In high-speed biological systems, specialized small muscles can rapidly trigger the release of energy stored by much larger, slower muscles (Gronenberg, 1995a,b; Patek 2011). For example, in the grasshopper, the small flexor tibiae muscle is used as a trigger for releasing energy generated by the much larger extensor tibiae muscle (Heitler, 1974). Similarly, in the alpheid shrimp, the dorsal closer muscle acts as a trigger for their extremely fast claw closing motion (Kaji et al., 2017). Similar small trigger muscles have also been hypothesized to be critical for the cicada jump (Gorb, 2004), the flea jump (with different small muscle triggers hypothesized in Bennet-Clark and Lucey, 1967 and Rothschild et al., 1972), and the mantid shrimp strike (Burrows, 1969; Patek et al., 2004). Thus, a wide variety of examples have been found in arthropods (reviewed in Gronenberg, 1996 and Patek et al., 2011).

Small muscles can also steer and control much larger muscles. The flight muscles of insects are large, but affect the wings only through indirect linkages; in contrast, small muscles directly insert on skeletal elements of the wing, and thus play critical roles in directing flight (Dickinson and Tu, 1997). Indeed, recent studies have shown that these muscles steadily induce small adjustments throughout flight by their tonic activity, whereas other small muscles can cause large and rapid directional changes through their phasic activity (Lindsay et al., 2017).

Finally, the passive properties of small muscles can affect limb positioning. In the locust, passive forces within the joint can generate flexion, whereas extension is driven by passive forces in the stick insect, because these muscles are adapted to the strengths of their antagonistic muscles (Ache and Matheson, 2013). Studies in locust leg demonstrated that the resting femur-tibia joint position was dependent on the history of prior activation of the large extensor tibiae muscle, again due to passive forces (Ache and Metheson, 2012). Moreover, passive forces are

dominant in small limbs, even in vertebrates such as mice, in which inertial forces are much smaller than passive forces (Hooper et al., 2009).

Mechanisms by which tongue-like structures acquire food

The arching of the surface by the sub-radular fibers during the protraction phase of biting and swallowing increases the likelihood that the radular surface will envelop seaweed, allowing the teeth on the radular surface to penetrate the seaweed as the radula retracts. In turn, the teeth enhance the ability of the radula to pull seaweed into the buccal cavity during the power stroke of swallowing, retraction (Ye et al., 2006; Lu et al., 2015). Because the teeth face posteriorly (towards the radular cleft), as the radular protracts, the teeth will disengage, allowing the radula to be positioned to grasp the next, more anterior part of the seaweed that the animal is ingesting.

Similar mechanisms have evolved to allow tongue-like structures to contact food, adhere to it, pull it into the oral cavity, and then release it. The high viscosity mucus secreted by the chameleon tongue allows the animal to ballistically extend its tongue and rapidly strike moving prey, such as a cricket, and hold onto the prey as it retracts the tongue (Brau et al., 2016), rather than propelling the prey away in response to the impulse force from the tongue. An analysis of the kinematics of frog tongues reveals that mucus on the tongue surface and the microscopic papillae on the tongue surface act together as a pressure-sensitive adhesive, assuring firm contact without the tongue peeling away from prey until it has been retracted into the oral cavity (Kleinteich and Gorb, 2015). In honeybees, erection of glossal hairs allows the tongue to trap nectar more effectively (Zhu et al., 2016). Cats (Reis et al., 2010) and dogs (Crompton and Musinsky, 2011) lap up fluids using inertial entrainment of the fluid in contact with the dorsal surface of the tongue. Thus, the exact details of the biomechanical solutions vary with the nature of the tongue-like structure, its speed of movement, and the properties of the material to be ingested, but each must address the critical problem of adhering to and drawing in food.

A novel mechanism for soft grasping

Understanding the detailed mechanisms by which soft-bodied animals are able to implement different behaviors has become a greater focus of interest as engineers and roboticists have begun to create artificial soft devices. A recent review focused on robots inspired by the locomotion of worms and caterpillars, as well as by the grasping capabilities of the octopus (Kim

et al., 2013). The engineering challenges for control, actuation, and fabrication are considerable, but great progress is being made by exploring many materials and control algorithms (Rus and Tolley, 2015; Laschi et al., 2016). An exciting new direction for soft robots and for robotics is the incorporation of biological materials directly into artificial devices - organismal engineering (Webster-Wood et al., 2017).

Creating soft grasping devices has been an area of intense interest for many years, as the rigid graspers characteristic of most robots are unable to handle fragile, soft and crushable materials. Investigators have explored the use of robots with soft fingers (Arimoto et al., 2000; Li and Kao, 2001; Or et al., 2016). A recent study used a topology optimization approach and three-dimensional printing to create a two-“finger” soft gripper that could handle a variety of fragile objects of differing sizes (Liu et al., 2018). Taking inspiration from invertebrates, other researchers created a robot that could locomote and grasp underwater, whose body design and function were inspired by the octopus (Cianchetti et al., 2015). A soft grasper was directly inspired by models of the buccal mass of *Aplysia* (Sutton et al., 2004b), and could grasp soft materials and transport them into a lumen using peristalsis (Mangan et al., 2005).

Grasping functions may differ depending on the goals of the organism. Studies of human grasping have distinguished between power grip (between the thumb and all the other fingers) and precision grip (between the index finger and the thumb), whose functions and neural substrates are different (Castiello, 2005). The power grip is to generate high forces on that object (for example, while climbing a branch) or for wielding a device (such as a hammer) to use it to exert significant forces on other objects. In contrast, the precision grip is used for fine manipulations, or for careful examination of an object. For a feeding system, such as that of *Aplysia*, the animal must also be able to use its grasper for multiple functions: to envelop and attach its radular surface to highly irregular, slippery and mechanically tough foods, and then to exert significant forces to snap off pieces so that the seaweed can be ingested.

Control of soft surfaces

How can the same soft surface be used for enveloping material, and then for generating the high forces necessary to break off pieces so that it can be swallowed? The biomechanical analysis of the way in which the radular surface can be arched and opened to envelop food, and then closed and retracted to exert strong forces that can break off pieces, is part of a larger area

of investigation — controlling the stiffness of soft materials, especially soft surfaces. A recent review focused on activation of soft structures arranged antagonistically, and of actuators whose elastic properties can be changed, to create controllable variable stiffness for robotic devices (Manti et al., 2016).

Other investigators have begun to focus on the control of the stiffness of thin sheets. The surface of the radula is flexible under compression, but does not undergo any significant expansion under tension in any direction (HJC and CEK, personal observations). An implication of Gauss's *Theorema Egregium* (“remarkable theorem”; Gauss, K.F., 1825, 1827) is that the *intrinsic curvature* of the radular surface will not change under deformation, so that if it is bent along one axis (e.g., the crease), the surface perpendicular to this direction will resist bending (become stiff), and this accounts for the ability of the sub-radular fibers to induce the sides of the surface on either side of the crease to bend away from the central crease, inducing opening. Similarly, compression of the edges of the radular sheet will induce arching of the surface. These phenomena can be observed in a thin sheet of paper subjected to curvature or to compressive forces along its sides, and analyses of these structures provide new insights into the development of structures with tunable stiffness (Callens and Zadpoor, 2018; Pini et al., 2016). Analysis of the geometric constraints on the responses of thin sheets have now become an important new area of investigation, and may lead to novel ways of deploying materials that are soft and have tunable stiffness (Marder et al., 2007; Li et al., 2012), as well as to the rational design of three-dimensional structures using concepts from origami and kirigami (Callens and Zadpoor, 2018). These concepts may also help clarify other areas of biology, such as the generation of complex morphologies during development depending on whether growth is conformal or generates internal stresses that cause the sheet of cells to assume a different three-dimensional shape (Irvine and Shraiman, 2017). The use of three-dimensional models similar to those developed for the analysis of the sub-radular fibers (Figure 8) may be a useful methodology for investigating these important questions.

Acknowledgements

We thank Jeffrey P. Gill, John P. Sasse, Gregory P. Sutton and two anonymous reviewers for their helpful comments on earlier drafts of the manuscript.

Competing Interests

The authors have no competing interests.

Funding

Research reported in this paper was supported by NSF grants DMS 1010434, IOS 1754869 and NIH grant NS047073 to HJC.

Data Availability

Data are available from Dryad at doi:10.5061/dryad.56r18rv; Blender files are available at GitHub at <https://github.com/tylikcat/slugmouths>.

References

Ache, J. M. and Matheson, T. (2013). Passive joint forces are tuned to limb use in insects and drive movements without motor activity. *Curr. Biol.* **23**, 1418-1426.

Ache, J. M. and Matheson, T. (2012). Passive resting state and history of antagonist muscle activity shape active extensions in an insect limb. *J. Neurophysiol.*, **107**, 2756-2768.

Arimoto, S., Nguyen, P. T. A., Han, H.-Y. and Doulgeri, Z. (2000) Dynamics and control of a set of dual fibers with soft tips. *Robotica* **18**, 71 – 80.

Bennet-Clark, H. C. and Lucey, E. C. A. (1967) The jump of the flea: A study of the energetics and a model of the mechanism. *J. exp. Biol.* **47**, 59 – 76.

Brau, F., Lanterbecq, D, Zghikh, L.-N., Bels, V. and Damman, P. (2016) Dynamics of prey prehension by chameleons through viscous adhesion. *Nature Physics* **12**, 931 – 935.

Burrows, M. (1969) The mechanics and neural control of the prey capture strike in the mantid shrimp *Squilla* and *Hemisquilla*. *Z. vergl. Physiologie* **62**, 361 – 381.

Carefoot, T. H. (1987) *Aplysia: Its Biology and Ecology*. In: *Oceanography and Marine Biology* **25**, (eds. H. Barnes and M. Barnes), pp. 139 – 249, Aberdeen, Scotland: Aberdeen University Press.

Castiello, U. (2005) The neuroscience of grasping. *Nature Rev. Neurosci.* **6**, 726 – 736.

Chiel, H. J. (2007) *Aplysia* feeding biomechanics. *Scholarpedia* **2**, 4165.

Chiel, H. J., Weiss, K. R., and Kupfermann, I. (1986) An identified histaminergic neuron modulates feeding motor circuitry in *Aplysia*. *J. Neurosci.* **6**, 2427 – 2450.

Cianchetti, M., Calisti, M, Margheri, L., Kuba, M. and Laschi, C. (2015) Bioinspired locomotion and grasping in water: the soft eight-arm OCTOPUS robot. *Bioinspir. Biomim.* **10**, 035003, 1 – 19.

Callens, S. J.P. and Zadpoor, A. A. (2018) From flat sheets to curved geometries: Origami and kirigami approaches. *Materials Today* **21**, 241 – 264.

Chow, S.-C., Shao, J., Wang, H. (eds.) (2008) *Sample Size Calculations in Clinical Research*, 2nd edition, 449 pp.

Clarke, C. L. (2004) The ecological role of sea hares (Opisthobranchia: Anaspeidea) within tropical intertidal habitats. M.S. Thesis, James Cook University, Townsville, Cairns, Australia.

Conn, H. J. (1953) *Biological stains: A handbook on the nature and uses of the dyes employed in the biological laboratory*. 6th edition. Biotech Publications, Geneva, NY.

- Crompton, A. W. and Musinsky, C. (2011) How dogs lap: ingestion and intraoral transport in *Canis familiaris*. *Biol. Lett.* **7**, 882 – 884.
- de Oliveira Saad, L., Cunha, C. M., Colpo, K.D., and Valdes, A. (2014) It's not what it looks like: molecular data fails to substantiate morphological differences in two sea hares (Mollusca, Heterobranchia, Aplysiidae) from southern Brazil. *Helgol. Mar. Res.* **68**:523–530.
- Dickinson, M. H. and Tu, M. S. (1997) The function of dipteran flight muscle. *Comp. Biochem. Physiol. A: Physiol.* **116**, 223 – 238.
- Duffy, J. E. and Hay, M. E. (1990) Seaweed adaptations to herbivory. *BioScience* **40**, 368 – 375.
- Evans, C. G., Rosen, S., Kupfermann, I., Weiss, K. R., and Cropper, E.C. (1996) Characterization of a radula opener neuromuscular system in *Aplysia*. *J. Neurophysiol.* **76**, 1267–1281. <https://doi.org/10.1152/jn.1996.76.2.1267>.
- Faul, F., Erdfelder, E., Buchner, A., and Lang, A.-G. (2009). Statistical power analyses using G*Power 3.1: Tests for correlation and regression analyses. *Behavior Research Methods*, **41**, 1149-1160.
- Gauss, K. F. General Investigations of Curved Surfaces of 1827 and 1825 (Disquisition generales circa superficies curvas). Translated with notes and a bibliography by Morehead, J. C. and Hildebrandt, A. M. (1902), Princeton University Library, 148 pages.
- Gorb, S. N. (2004) The jumping mechanism of cicada *Cercopis vulnerata* (Auchenorrhyncha, Cercopidae): skeleton-muscle organization, frictional surfaces, and inverse-kinematic model of leg movements. *Arthropod Struct. Develop.* **33**, 201 – 220.
- Gronenberg, W. (1995a) The fast mandible strike in the trap-jaw ant *Odontomachus*: I. Temporal properties and morphological characteristics. *J. Comp. Physiol. A* **176**, 391 – 398.
- Gronenberg, W. (1995b) The fast mandible strike in the trap-jaw ant *Odontomachus*: II. Motor Control. *J. Comp. Physiol. A* **176**, 399 – 408.
- Gronenberg, W. (1996) Fast actions in small animals: springs and click mechanisms. *J. Comp. Physiol. A* **178**, 727 – 734.
- Hay, M. E. (1997) The ecology and evolution of seaweed-herbivore interactions on coral reefs. *Coral Reefs* **16**, Suppl. S67-S76.
- Heitler, W. J. (1974) The locust jump: Specialisations of the metathoracic femoral-tibial joint. *J. Comp. Physiol.* **89**, 93 – 104.

Hooper, S. L., Guschlbauer, C., Blümel, M., Rosenbaum, P., Gruhn, M., Akay, T., and Büschges, A. (2009). Neural control of unloaded leg posture and of leg swing in stick insect, cockroach, and mouse differs from that in larger animals. *J. Neurosci.*, **29**, 4109-4119.

Hooper, S.L., Hobbs, K.H. and Thuma, J.B. (2008) Invertebrate muscles: Thin and thick filament structure; molecular basis of contraction and its regulation, catch and asynchronous muscle. *Prog. Neurobiol.* **86**:72–127.

Hooper, S.L and Thuma, J.B. (2005) Invertebrate muscles: Muscle specific genes and proteins. *Physiol Rev* **85**:1001–1060.

Howells, H. H. (1942) The structure and function of the alimentary canal of *Aplysia punctata*. *J. Cell Sci.* **s2-83**, 357 – 397.

Humason, G.L. (1979). *Animal Tissue Techniques*. 4th ed. San Francisco: W.H. Freeman.

Hurwitz, I. and Susswein, A. J. (1992) Adaptation of feeding sequences in *Aplysia oculifera* to changes in the load and width of food. *J. exp. Biol.* **166**, 215 -235.

Hurwitz, I., Neustadter, D., Morton, D. W., Chiel, H. J. and Susswein, A. J. (1996) Activity patterns of the B31/B32 pattern initiators innervating the I2 muscle of the buccal mass during normal feeding movements in *Aplysia californica*. *J. Neurophysiol.* **75**, 1309 – 1326.

Irvine, K. D. and Shraiman, B. I. (2017) Mechanical control of growth: ideas, facts and challenges. *Development* **144**, 4238 – 4248.

Kaji, T., Anker, A., Wirkner, C. S. and Palmer, A. R. (2018) Parallel saltational evolution of ultrafast movements in snapping shrimp claws. *Curr. Biol.* **28**, 106 – 113.

Katzoff, A., Ben-Gedalya, I., Hurwitz, N., Miller, Y. Z., and Susswein, A. J. (2006) Nitric oxide signals that *Aplysia* have attempted to eat, a necessary component of memory formation after learning that food is inedible. *J. Neurophysiol.* **96**, 1247 – 1257.

Kim, S., Laschi, C. and Trimmer, B. (2013) Soft robotics: A bioinspired evolution in robotics. *Trends Biotech.* **31**, 287 – 294.

Kleinteich, T. and Gorb, S. N. (2015) Frog tongue acts as muscle-powered adhesive tape. *Roy. Soc. Open Sci.* **2**: 150333, 1 – 9, doi: <http://dx.doi.org/10.1098/rsos.150333>.

Kupfermann, I. (1974) Feeding behavior in *Aplysia*; A simple system for the study of motivation. *Behav. Biol.* **10**, 1 – 26.

Kupfermann, I. and Carew, T. J. (1974) Behavior patterns of *Aplysia californica* in its natural environment. *Behav. Biol.* **12**, 317 – 337.

Laschi, C., Mazzolia, B., and Cianchetti, M. (2016) Soft robotics: Technologies and systems pushing the boundaries of robot abilities. *Sci. Robot.* **1**, eaah3690, 1 – 11.

Li, B., Cao, Y.-P., Feng, X.-Q. and Gao, H. (2012) Mechanics of morphological instabilities and surface wrinkling in soft materials: a review. *Soft Matter* **8**, 5728 – 5745.

Li, Y. and Kao, I. (2001) A review of modeling of soft-contact fingers and stiffness control for dexterous manipulation in robotics. *Proc. 2001 Int. Conf. Robot. Automat.* Seoul, Korea, May 21 – 26, 3055 – 3060.

Lindsay, T., Suster, A., Dickinson, M. (2017) The function and organization of the motor system controlling flight maneuvers in flies. *Curr. Biol.* **27**, 345 – 358.

Liu, C.-H., Chen, T.-L., Chiu, C.-H., Hsu, M.-C., Chen, Y., Pai, T.-Y., Peng, W.-G. and Chiang, Y.-P. (2018) Optimal design of a soft robotic gripper for grasping unknown objects. *Soft Robotics* **5**, 452 – 465.

Lu, H., McManus, J. M., Cullins, M. J. and Chiel, H. J. (2015) Preparing the periphery for a subsequent behavior: Motor neuronal activity during biting generates little force but prepares a retractor muscle to generate larger forces during swallowing in *Aplysia*. *J. Neurosci.* **35**, 5051 – 5066.

Mangan, E. V., Kingsley, D. A., Quinn, R. D., Sutton, G. P., Mansour, J. M. and Chiel, H. J. (2005). A biologically inspired gripping device. *Industrial Robot: An International Journal* **32**, 49 – 54.

Manti, M., Cacucciolo, V. and Cianchetti, M. (2016) Stiffening in soft robotics: A review of the state of the art. *IEEE Robot. Automat. Mag.* September 2016, 93 – 106, doi: 10.1109/MRA.2016.2582718.

Marder, M., Deegan, R. D. and Sharon, E. (2007) Crumpling, buckling and cracking: Elasticity of thin sheets. *Physics Today*, February 2007, 33 – 38.

Morton, D. W. and Chiel, H. J. (1993) *In vivo* buccal nerve activity that distinguishes ingestion from rejection can be used to predict behavioral transitions in *Aplysia*. *J. Comp. Physiol. A* **172**, 17 – 32.

Neustadter, D. M., Drushel, R. F. and Chiel, H. J. (2002a) Kinematics of the buccal mass during swallowing based on magnetic resonance imaging in intact, behaving *Aplysia californica*. *J. exp. Biol.* **205**, 939 - 958.

Neustadter, D. M., Drushel, R. F., Crago, P. E., Adams, B. W., and Chiel, H. J. (2002b) A kinematic model of swallowing in *Aplysia californica* based on radula/odontophore kinematics and *in vivo* magnetic resonance images. *J. exp. Biol.* **205**, 3177–3206.

Neustadter, D. M., Herman, R.L., Drushel, R.F., Chestek, D. W. and Chiel, H.J. (2007) The kinematics of multifunctionality: Comparisons of biting and swallowing in *Aplysia californica*. *J. Exp. Biol.* **210**, 238–260. <https://doi.org/10.1242/jeb.02654>.

Novakovic, V. A., Sutton, G. P., Neustadter, D. M., Beer, R. D. and Chiel, H. J. (2006) Mechanical reconfiguration mediates swallowing and rejection in *Aplysia californica*. *J. Comp. Physiol. A* **192**, 857 – 870.

Or., K., Morikuni, S., Ogasa, S., Funabashi, S., Schmitz, A. and Sugano, S. (2016) A study on fingertip designs and their influences on performing stable prehension for robot hands. 2016 IEEE-RAS 16th International Conference on Humanoid Robots (Humanoids), Cancun, Mexico, Nov. 15 – 17, 2016, 772 – 777.

Orehkova, I. V., Jing, J., Brezina, V., DiCaprio, R. A., Weiss, K. R. and Cropper, E. C. (2001) Sonometric measurements of motor-neuron-evoked movements of an internal feeding structure (the radula) in *Aplysia*. *J. Neurophysiol.* **86**, 1057-1061.

Patek, S.N., Korff, W. L. and Caldwell, R.L. (2004) Biomechanics: Deadly strike mechanisms of a mantis shrimp. *Nature* **428**, 819 – 820.

Patek, S.N., Baio, J. E., Fisher, B.L., Suarez, A. V. (2006) Multifunctionality and mechanical origins: Ballistic jaw propulsion in trap-jaw ants. *Proc. Nat. Acad. Sci. (USA)* **103**, 12787 – 12792.

Patek, S. N., Dudek, D. M. and M. V. Rosario, M. V. (2011) From bouncy legs to poisoned arrows: elastic movements in invertebrates. *J. exp. Biol.* **214**, 1973 – 1980.

Pennings, S. C. (1990) Size-related shifts in herbivory: specializing in the sea hare *Aplysia californica* Cooper. *J. Exp. Mar. Biol. Ecol* **142**, 43 – 61.

Pini, V., Ruz, J. J., Kosaka, P. M., Malvar, O., Calleja, M. and Tamajo, J. (2016) How two-dimensional bending can extraordinarily stiffen thin sheets. *Sci. Reports* **6**, 29627, 1 – 6, doi: 10.1038/srep29627.

Reis, P. M., Jung, S., Aristoff, J. M. and Stocker, R. (2010) How cats lap: Water uptake by *Felis catus*. *Science* **330**, 1231 – 1234.

Rothschild, M., Schlein, Y., Parker, K. and Sternberg, S. (1972) Jump of the oriental rat flea *Xenopsylla cheopis* (Roths.) *Nature* **239**, 45 – 48.

Rus, D. and Tolley, M. T. (2015) Design, fabrication and control of soft robots. *Nature* **521**, 467 – 475.

Steneck, R. S. and Watling, L. (1982) Feeding capabilities and limitation of herbivorous molluscs: a functional group approach. *Mar. Biol.* **68**, 299 – 319.

Susswein, A. J., Rosen, S. C., Gapon, S. and Kupfermann, I. (1996) Characterization of buccal motor programs elicited by a cholinergic agonist applied to the cerebral ganglion of *Aplysia californica*. *J. Comp. Physiol. A* **179**, 509 – 524.

Sutton, G. P., Macknin, J. B., Gartman, S.S., Sunny, G. P., Beer, R. D., Crago, P. E., Neustadter, D. M. and Chiel, H. J. (2004a) Passive hinge forces in the feeding apparatus of *Aplysia* aid retraction during biting but not swallowing. *J. Comp. Physiol. A* **190**, 501 – 514.

Sutton, G. P., Mangan, E. V., Neustadter, D. M., Beer, R. D., Crago, P. E. and Chiel, H. J. (2004b) Neural control exploits changing mechanical advantage and context dependence to generate different feeding responses in *Aplysia*. *Biol. Cyber.* **91**, 333 – 345.

Trowbridge, C. D. (1997) Dietary induction of opisthobranch morphology: *Placida dendritica* (Alder & Hancock, 1843) on different green algal hosts. *J. Moll. Stud.* **63**, 29 – 38.

Winkler, L. R. and Dawson, E. Y. (1963) Observations and experiments on the food habits of California sea hares of the genus *Aplysia*. *Pacific Science* **17**, 102 – 105.

Ye, H., Morton, D. W., and Chiel H. J. (2006) Neuromechanics of coordination during swallowing in *Aplysia californica*. *J. Neurosci.* **26**, 1470 – 1485.

Zhu, R., Lv, H., Liu, T., Yang, Y., Wu, J. and Yan, S. (2016) Feeding kinematics and nectar intake of the honey bee tongue. *J. Insect Behav.* **29**, 325 – 339.

Figures

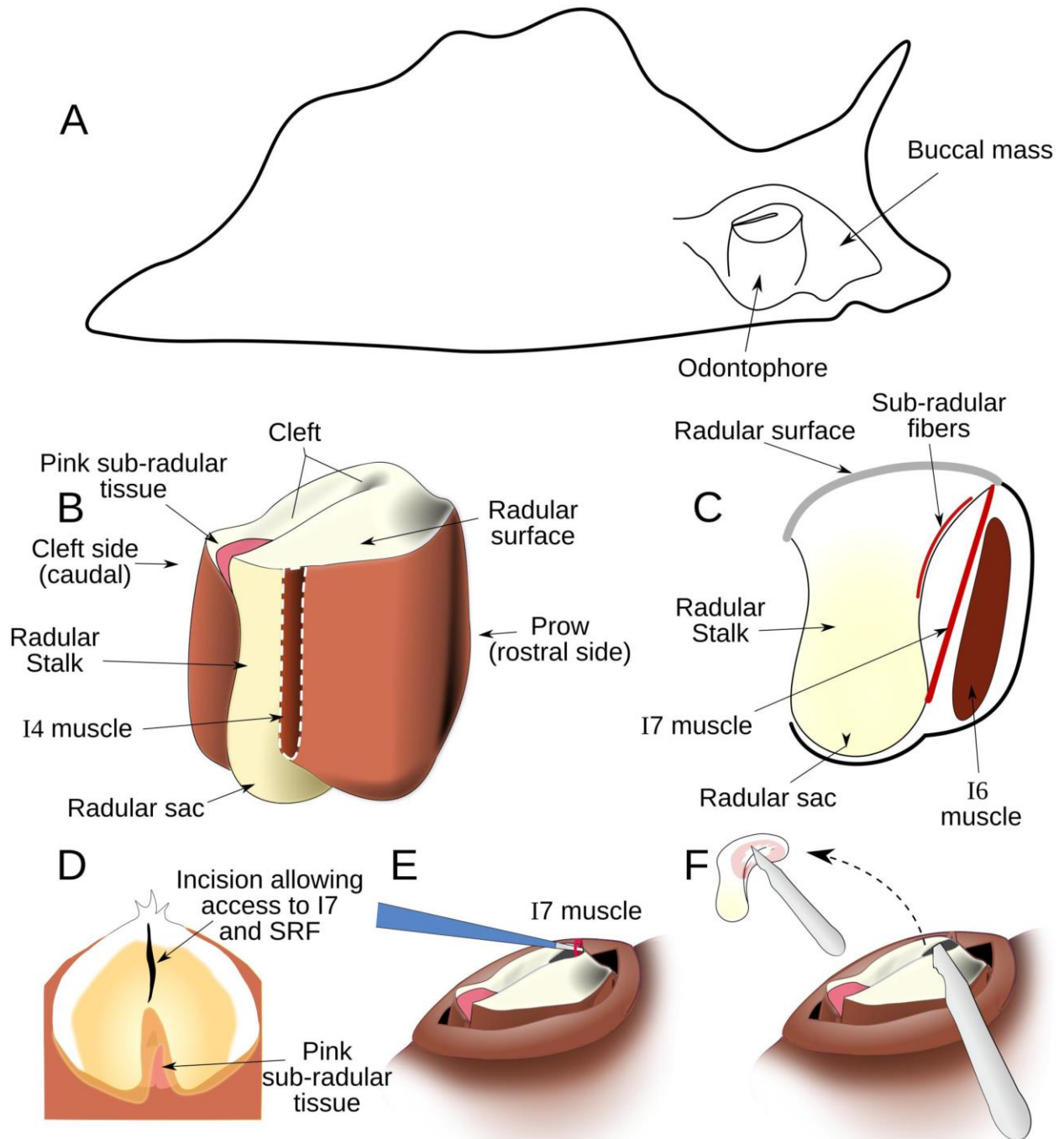


Figure 1. Anatomy and *in vivo* surgery. A. Schematic location of the feeding apparatus (buccal mass) within an animal's body. B. Schematic external view of radular surface, radular base, radular sac, and odontophore muscles. The I4 muscle is removed (white dashed line) to show the radular stalk. C. Schematic mid-sagittal view, showing locations of muscles I6, I7, and the sub-radular fibers relative to the radular surface. The leaflets of the I5 muscle (not shown in the schematic) insert along the lateral sides of the radular stalk, and do not overlap the sub-radular fibers. The sub-radular fibers are distinct from the pink sub-radular tissue. D. Schematic view of the initial surgical incision in the surface of the radula to gain access to the I7 muscle and the sub-radular fibers. E. Schematic view of removal of an I7 muscle. F. Schematic view of removal of sub-radular fibers; the small inset schematically indicates the extent of their removal (about 2/3 of the fibers).

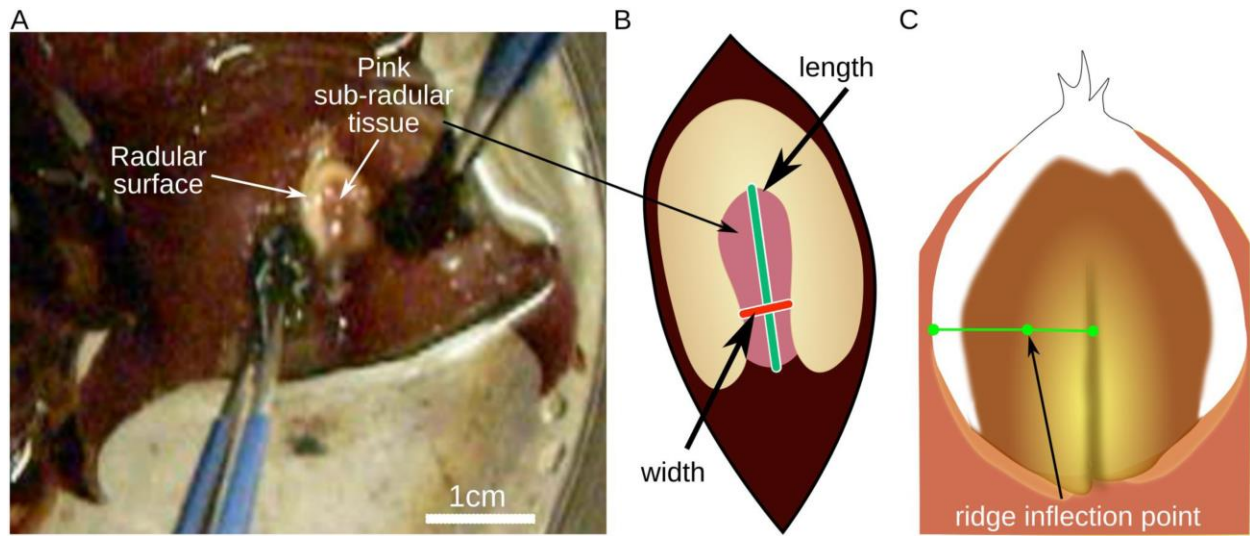


Figure 2. Measurement of opening width during biting behavior. A. Seaweed applied to both sides of the peri-oral zone induced strong, regular bites. B. Opening width was normalized by the length of the radular cleft. C. As a proxy for measuring radular surface curvature, the curvature exclusion was determined by measuring the distance from the ridge inflection point to the center of the radula, normalized by the length from edge to center of the radular surface.

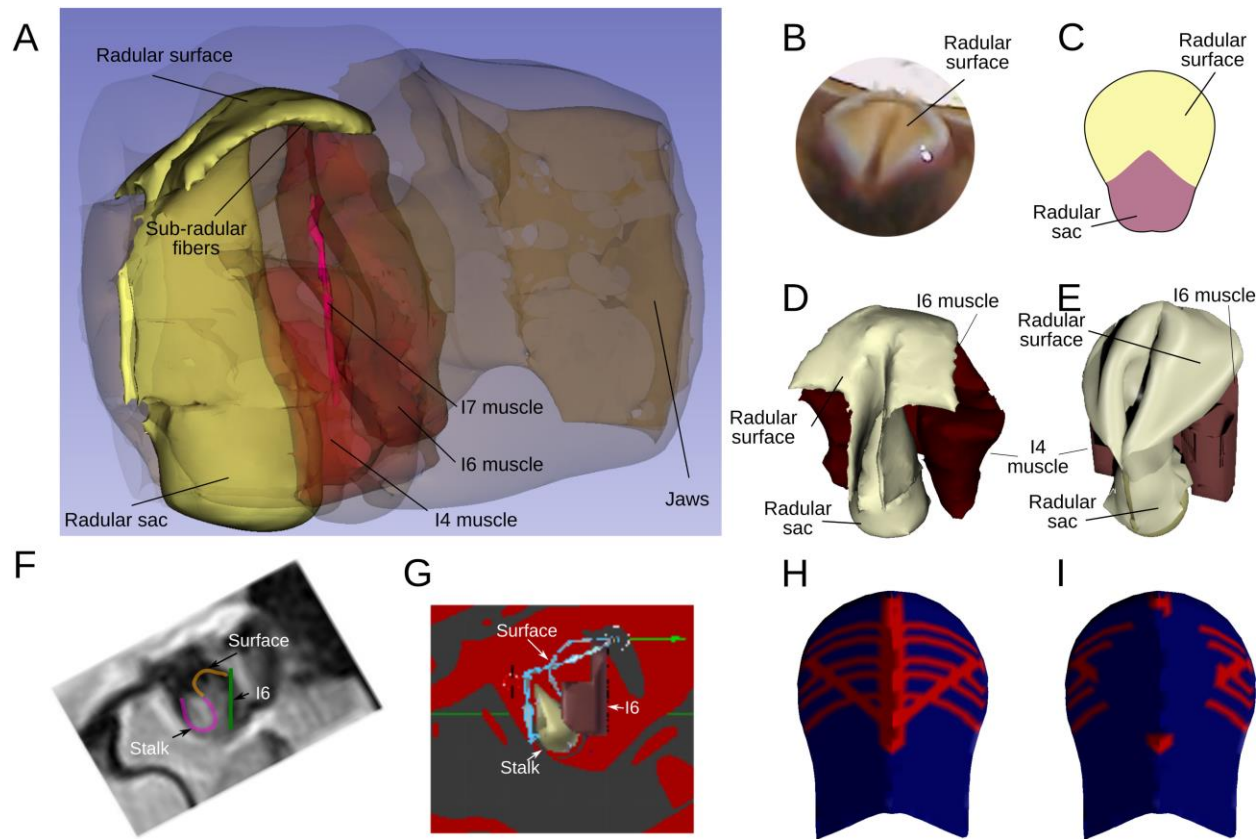


Figure 3. Soft radular surface model. A. Reconstruction of the entire buccal mass based on high-spatial-resolution MRI provided initial resting positions for the muscles beneath the radular surface. B. A dorsal view of the radular surface. C. Schematic of the flattened radular surface. D. Static image of the radular surface and underlying tissues extracted from the high-spatial-resolution MRI model (panel A). E. Simplification of the structure of the I4/I6 complex (red mesh). F. Location of structures during biting from a high-temporal-resolution MRI video frame. G. Radular surface (blue line) is fitted to the model structures (based on MRI, panel F). H. Vertex group representing sub-radular fibers (see text). I. Lesion of sub-radular fibers (see text).

A Radular surface, no I7 muscles



B Radular opening, no I7 muscles

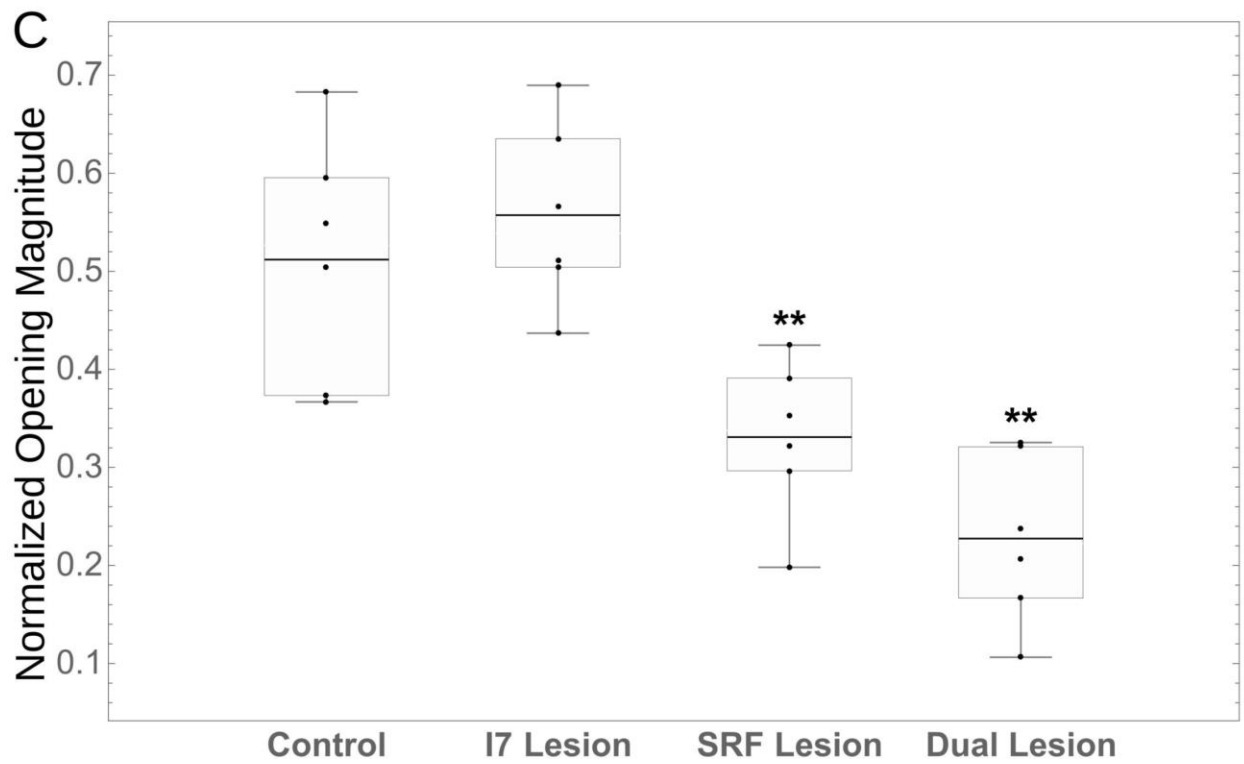
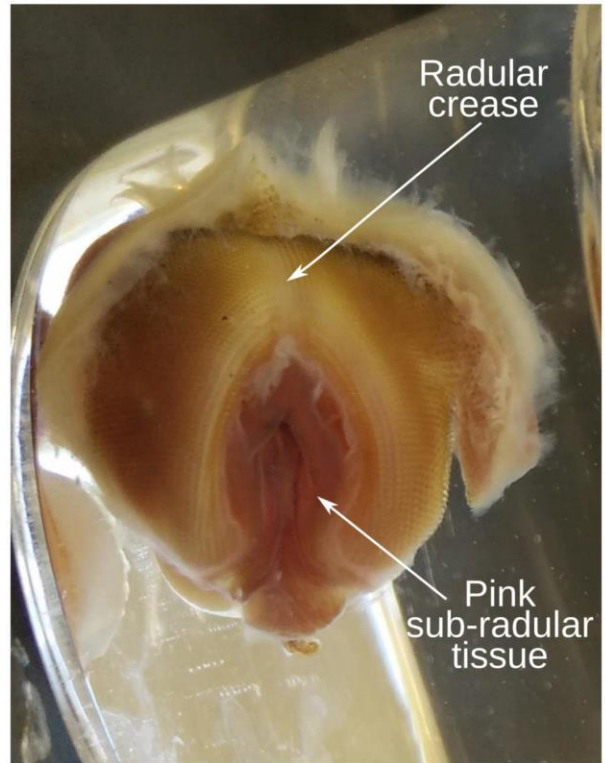


Figure 4. Sub-radular fibers contribute to opening *in vitro* in the absence of the I7 muscles. A. Reduced preparation for studying opening *in vitro*. The I7 muscles have been removed. B. Large radular opening induced by carbachol. C. Comparison of effects of control, I7 lesion, SRF lesion, and dual lesions. Overall ANOVA was highly significant ($F(3, 20) = 15.07$, $p < 0.000023$). SRF lesion and dual lesions are highly significant when compared to control lesions and I7 lesions; no other differences are significant. Normalized openings were 0.51 ± 0.12 , whereas the normalized opening values for the I7 lesioned group were 0.55 ± 0.09 (mean \pm s.d., $N = 6$ preparations for both groups). Normalized opening values for the SRF lesioned group were 0.33 ± 0.08 ($N = 6$ preparations; $p < 0.03$, Tukey HSD post-hoc test comparing SRF lesion to control group). The normalized opening values for the dual lesioned group were 0.23 ± 0.09 ($N = 6$ preparations; $p < 0.0003$, Tukey HSD post-hoc test comparing dual lesion to control). The middle line in each box represents the mean; top and bottom whiskers correspond to maximum and minimum values; top and bottom of each box correspond to the third and first quartiles, respectively. The original data points are shown as dots. These conventions apply to the box and whisker plots in Figure 6.

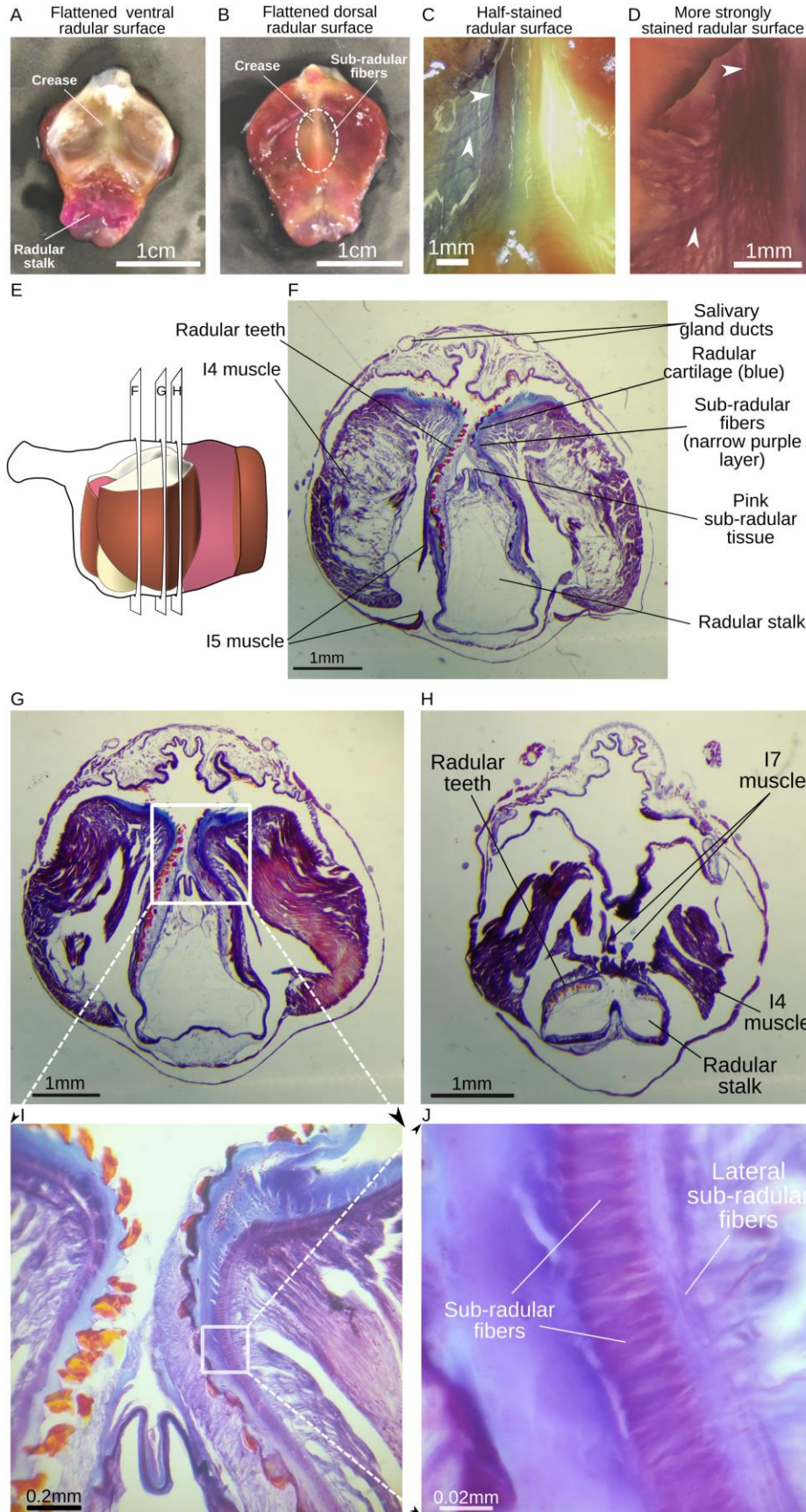


Figure 5. Anatomy and histology of the sub-radular fibers. A. Ventral view of flattened radular surface and crease. B. Dorsal view showing location of sub-radular fibers relative to the central crease. C. Lightly stained ventral surface (see Methods), showing longitudinal and perpendicular fibers (white arrows). D. Density of sub-radular fibers is clear after heavy staining (see Methods). E. Schematic side view of the buccal mass, indicating locations of the sections through the buccal mass shown in panels F, G, and H. F. A 20 μm thin section of the buccal mass, showing the very thin layer of sub-radular fibers immediately beneath the cartilage of the radula and its teeth. G. A more anterior section in which the course of the sub-radular fibers can be followed more clearly. H. A still more anterior section which shows part of the I7 muscles in cross-section. I. Further magnification of section G (indicated by box), showing the position of the sub-radular fibers relative to the cartilage of the radula and its teeth. J. Magnification of section in I (indicated by box) showing the tight packing of the sub-radular fibers, and the course of the perpendicular lateral sub-radular fibers.

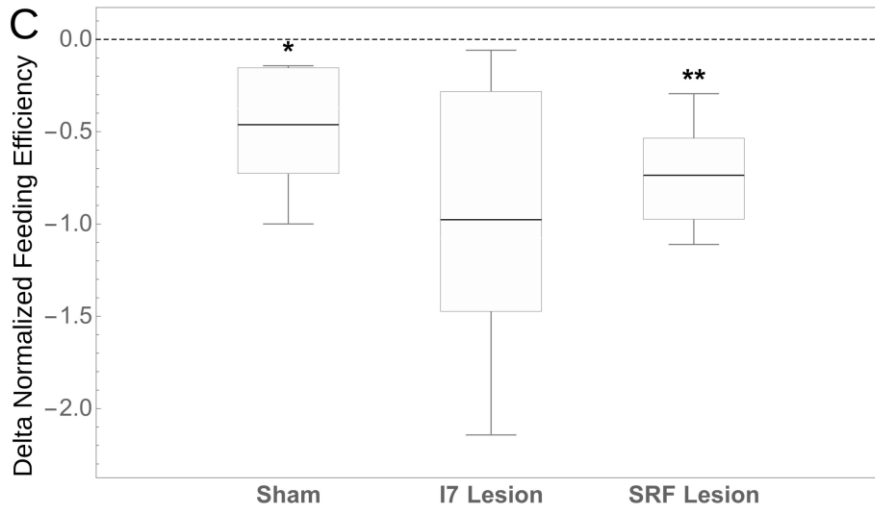
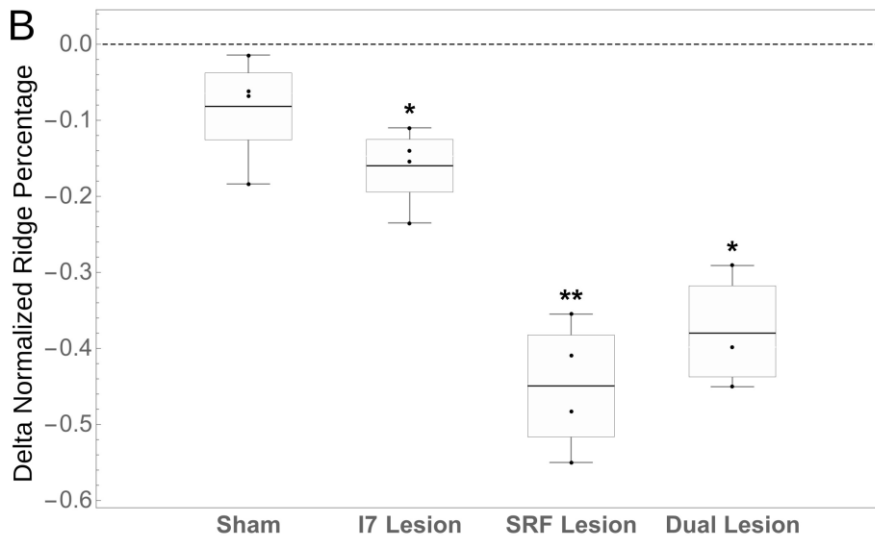
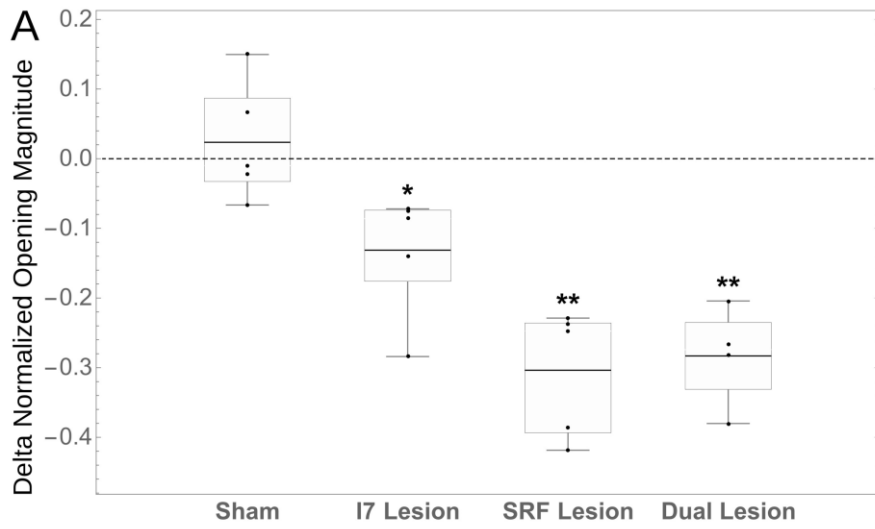


Figure 6. I7 and sub-radular fiber lesions reduce radular opening and arching *in vivo*, and SRF lesions reduce feeding efficiency. A. Effect of lesions (sham, I7, SRF, or SRF and I7 lesions) on normalized opening magnitude. Data show differences of means for each of five animals before and after lesions (animals served as their own controls; see Methods). Difference of means pre-sham surgery vs. post-sham surgery, 0.024 ± 0.085 , mean \pm s.d., not significant, N = 5 animals (5 bites from each); effect size = 0.28. Pre-I7 lesion vs. post-I7 lesion, -0.13 ± 0.09 , $p < 0.031$, paired t-test, N = 5 animals (5 bites from each); effect size = -1.4. Pre-SRF lesion vs. post-SRF lesion, -0.30 ± 0.091 , $p < 0.0017$, paired t-test, N = 5 animals (5 bites from each); effect size = -3.3. Pre-dual lesions vs. post-dual lesions, -0.28 ± 0.073 , $p < 0.0044$, paired t-test, N = 4 animals (5 bites from each); effect size = -3.8. Note that the effect size of either the SRF or of the dual lesions is larger than the effect size of lesioning I7 alone. B. Effect of the same lesions on normalized ridge formation, again showing differences of means (N = 4 animals in sham, I7 and SRF groups, N = 3 in dual lesion group). Pre-sham surgery vs. post-sham surgery, -0.082 ± 0.072 , $p > 0.1$ (n.s.), N = 4 animals (4 bites from each); effect size = -1.14. Pre-I7 lesion vs. post-I7 lesion, -0.16 ± 0.05 , $p < 0.01$, paired t-test, N = 4 animals (4 bites from each); effect size = -3.2. SRF lesions alone: -0.45 ± 0.085 , $p < 0.0019$, paired t-test, N = 4 animals (4 bites from each); effect size = -5.3. Dual lesions: -0.38 ± 0.081 , $p < 0.015$, paired t-test, N = 3 animals (4 bites from each); effect size = -4.7. Note that the effect size of SRF or dual lesions is larger than the effect size of lesioning I7 alone. C. Effects of sham, I7 and SRF lesions on feeding efficiency. Differences in mean number of swallows, pre-sham vs. post-sham surgery, normalized by pre-sham mean swallows, -0.46 ± 0.36 , $p < 0.046$, paired t-test, N = 5; effect size = -1.3. Pre-I7 minus post-I7 lesions, -0.98 ± 0.82 , $p = 0.056$, paired t-test, N = 5; effect size = -1.2. Pre-SRF minus post-SRF lesions, -0.74 ± 0.31 , $p < 0.0062$, paired t-test, N = 5; effect size = -2.4. Note that the effect size of the SRF lesion is larger than that of either the sham or I7 lesions.

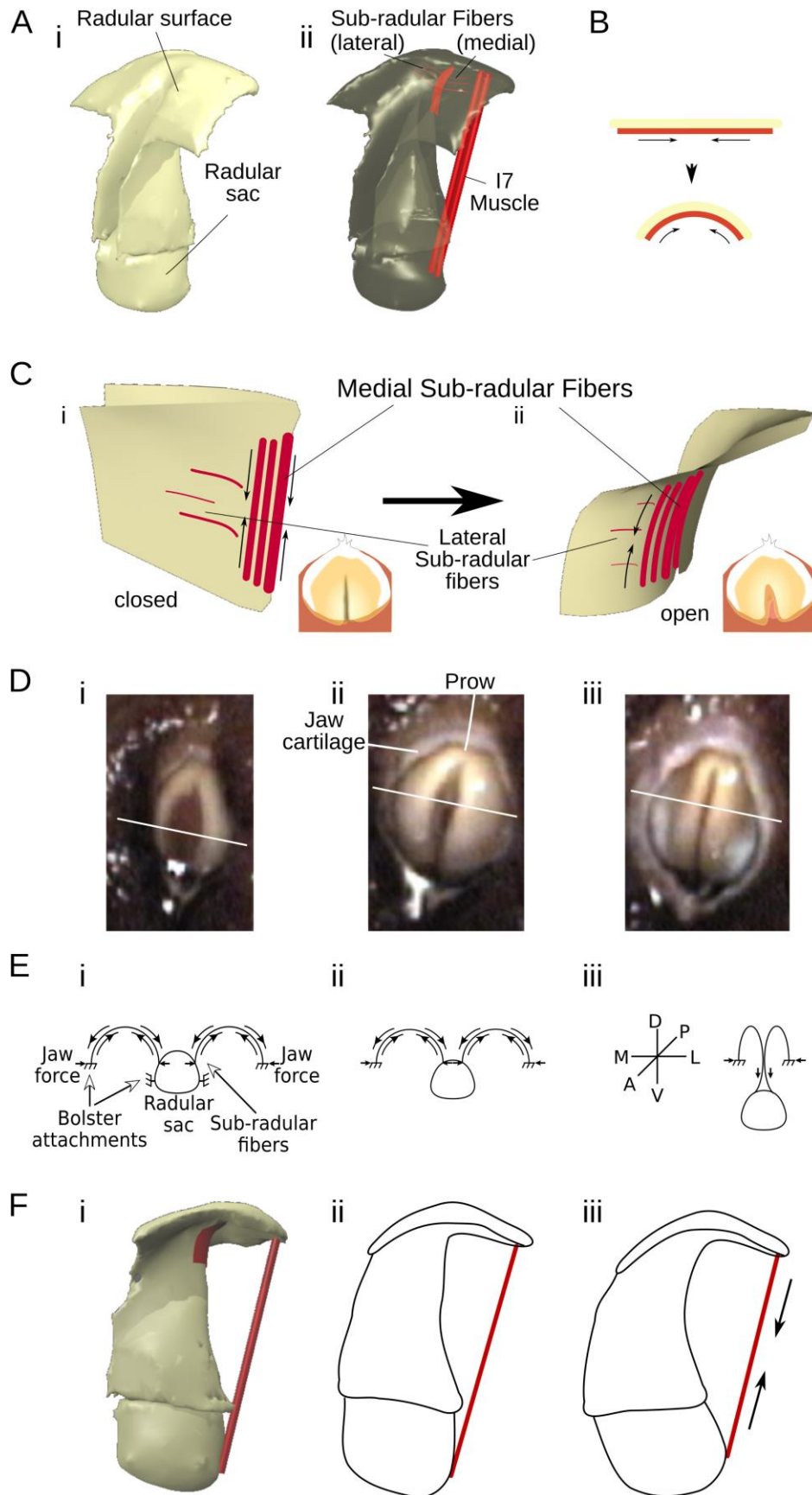


Figure 7. Biomechanics of the actions of the sub-radular fibers and the I7 muscles. A. i. Three-dimensional view of radular surface, stalk and sac. ii. Location of sub-radular fibers and I7 muscles that contribute to opening are highlighted in red. B. Schematic indicating compressive actions of sub-radular fibers that induce outward curvature of radular surface. C. Stiff crease in radular surface induces sub-radular fibers (shown in panel i) to curve radular surface away from crease, causing opening (panel ii). Insets show top view of radular surface. D. i. Video frame of early protraction of biting in an intact animal. ii. Video frame of peak protraction during the same bite; the opening of the radular halves and their gentle curvature is clearly visible. iii. Video frame at the onset of retraction during the same bite. The central stiff ridge is clearly visible. E. Schematics shown below the video frames are oriented such that the radular surface is dorsal, the radular sac is ventral, the prow is posterior, and the radular cleft is anterior. White lines across the surface of the radula in each video frame indicate the “cross-section” represented by the schematic drawing. Solid arrows represent forces. i. Early protraction. ii. Peak protraction. iii. Onset of retraction and ridge formation. See text. F. First panel (i) shows the location of I7 muscles relative to the radular surface and the radular sac. As the I7 muscles contract (panel ii), they pull the radular surface apart and also induce the radular stalk to move towards the radular surface (panel iii).

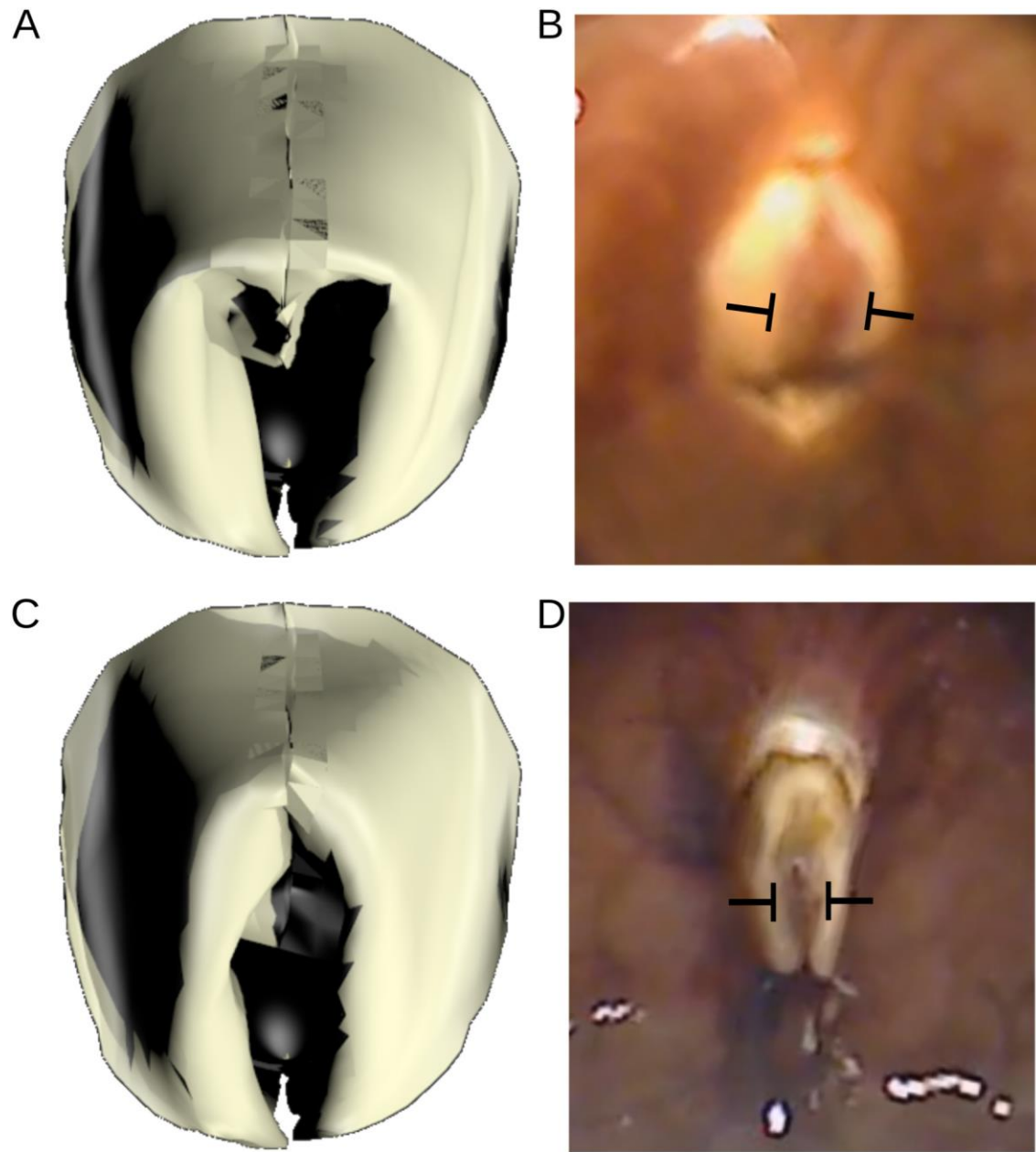


Figure 8. Model replicates effects of SRF lesion. A. Peak protraction, sub-radular fibers stiffened; this generates a normal bite. B. *In vivo* video frame of peak protraction in an unlesioned animal. C. Peak protraction, sub-radular fibers not stiffened; opening is significantly reduced. D. Video frame of *in vivo* peak bite in the same animal as in part B after lesion of sub-radular fibers.

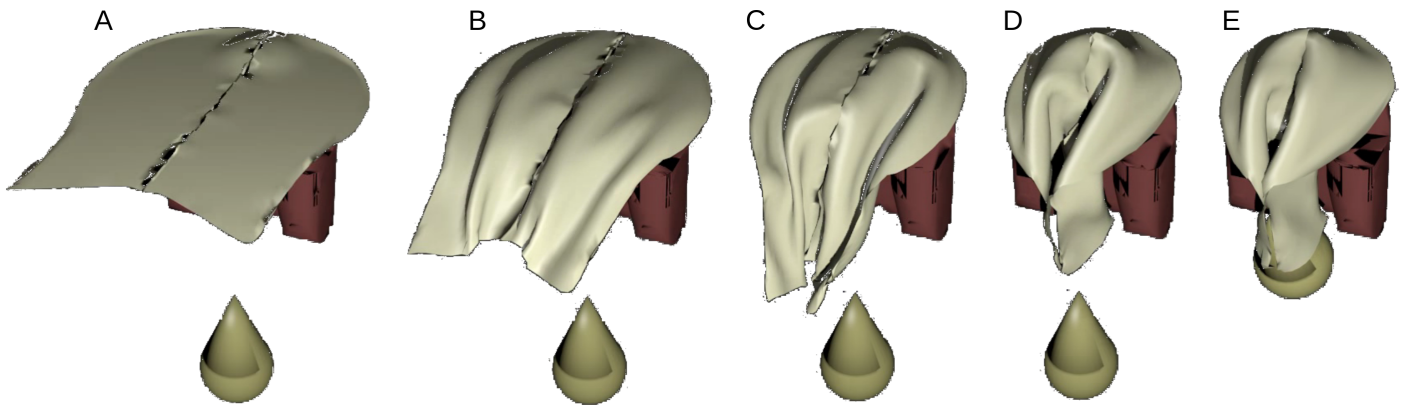
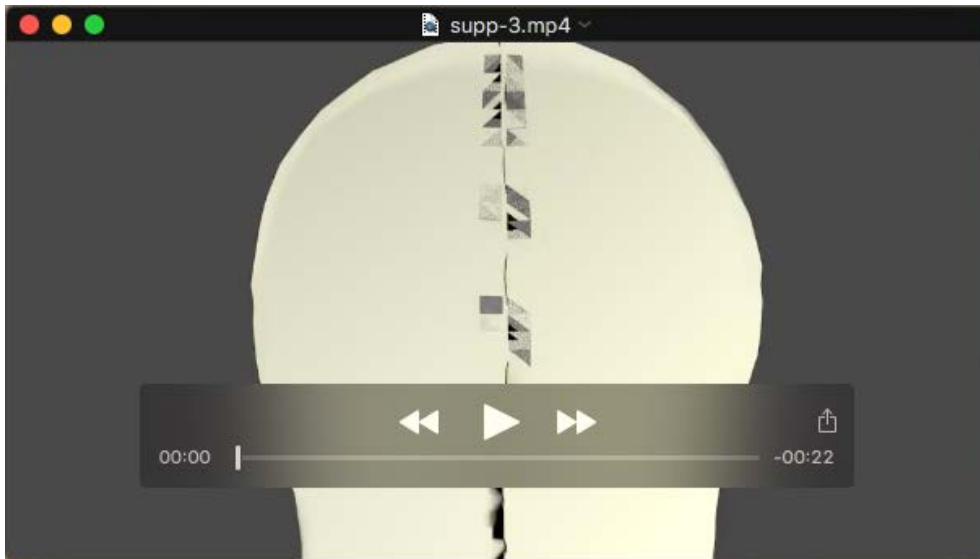
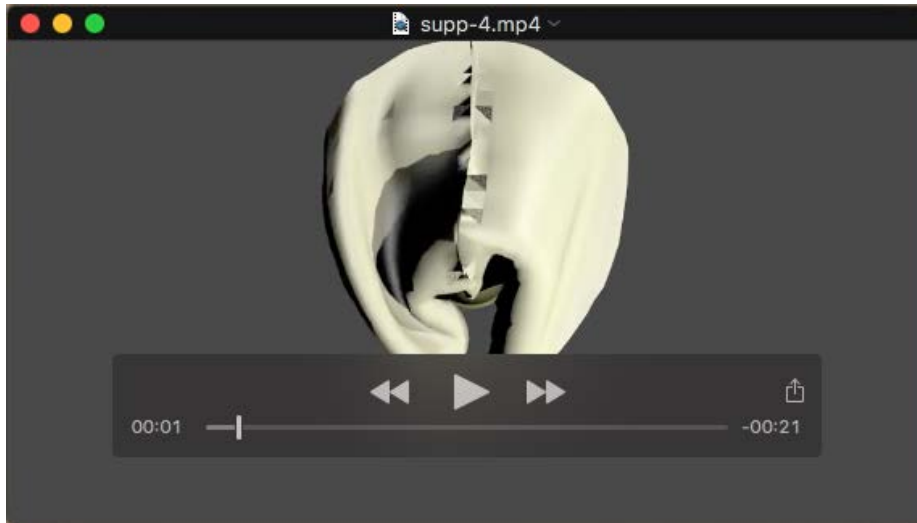


Figure S1. Assembly of radular surface and radular sac. A. Initial position of radular surface; radular sac is beneath it. B. - D. Process of folding radular surface. E. Radular sac is moved upwards into the base of the radular stalk.



Movie 1 (LSRFTri.ogg): Assembly of model, and then three successive bites in which the lateral sub-radular fibers are activated, showing the normal pattern of biting, including large openings near the peak of protraction, followed by ridge formation and retraction.



Movie 2 (LSRFLesionTri.ogg): Assembly of model, and then three successive bites in which the lateral sub-radular fibers are not activated. Opening is much smaller, and ridge formation is weaker.



Movie 3 (LSRFInverseTri.ogg): Assembly of model, and then three successive bites in which the lateral sub-radular fibers are activated at times that are passive in intact animals. The three bites are severely disrupted.

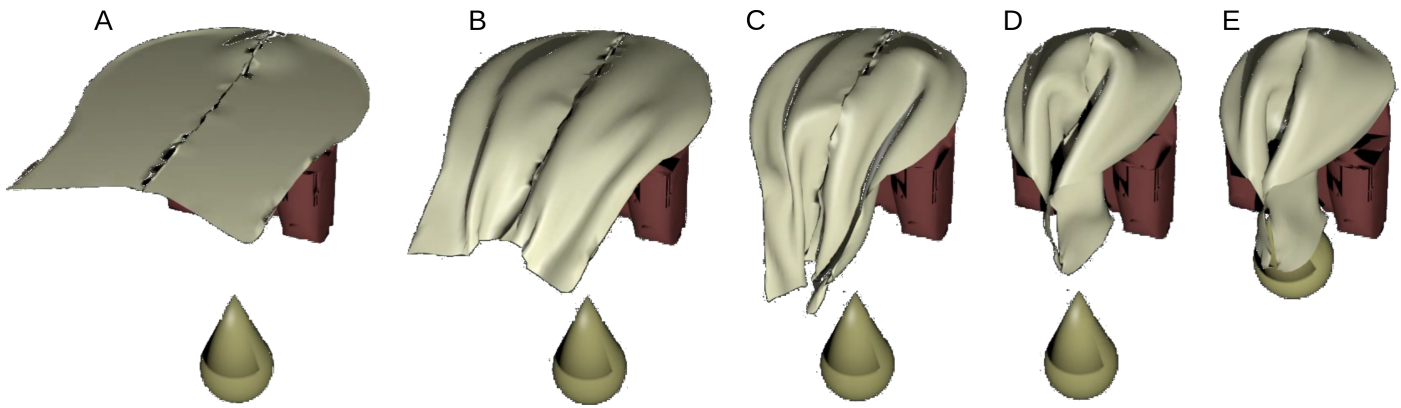
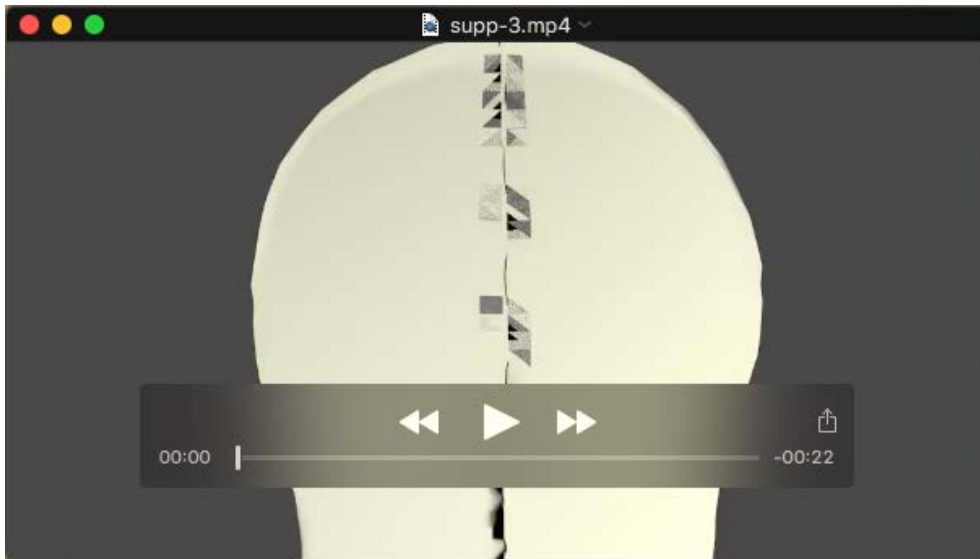


Figure S1. Assembly of radular surface and radular sac. A. Initial position of radular surface; radular sac is beneath it. B. - D. Process of folding radular surface. E. Radular sac is moved upwards into the base of the radular stalk.



Movie 1 (LSRFTri.ogg): Assembly of model, and then three successive bites in which the lateral sub-radular fibers are activated, showing the normal pattern of biting, including large openings near the peak of protraction, followed by ridge formation and retraction.



Movie 2 (LSRFLesionTri.ogg): Assembly of model, and then three successive bites in which the lateral sub-radular fibers are not activated. Opening is much smaller, and ridge formation is weaker.



Movie 3 (LSRFInverseTri.ogg): Assembly of model, and then three successive bites in which the lateral sub-radular fibers are activated at times that are passive in intact animals. The three bites are severely disrupted.